Aerospace Science and Technology, Volume 60, January 2017, pp. 84-95
DOI:10.1016/j.ast.2016.11.001

Accepted Manuscript

Jetstream 31 national flying laboratory: Lift and drag measurement and modelling

N.J. Lawson, H. Jacques, J.E. Gautrey, A.K. Cooke, J.C. Holt, K.P. Garry

PII: S1270-9638(16)30338-8
DOI: http://dx.doi.org/10.1016/j.ast.2016.11.001
Reference: AESCTE 3818

To appear in: *Aerospace Science and Technology*

Received date: 27 July 2016
Accepted date: 3 November 2016

Please cite this article in press as: N.J. Lawson et al., Jetstream 31 national flying laboratory: Lift and drag measurement and modelling, *Aerosp. Sci. Technol.* (2016), http://dx.doi.org/10.1016/j.ast.2016.11.001

Aerospace Science and Technology

Jetstream 31 National Flying Laboratory: Lift and Drag Measurement and Modelling

N J Lawson, H Jacques, J E Gautrey, A K Cooke, J C Holt, K P Garry

National Flying Laboratory Centre, Cranfield University
Cranfield, Bedfordshire. MK43 0AL
Tel: 01234 758245 Fax: 01234 758207
Email: n.lawson@cranfield.ac.uk

Abstract:

Lift and drag flight test data is presented from the National Flying Laboratory Centre, Jetstream 31 aircraft. The aircraft has been modified as a flying classroom for completing flight test training courses, for engineering degree accreditation. The straight and level flight test data is compared to data from 10% and 17% scale wind tunnel models, a Reynolds Averaged Navier Stokes steady-state computational fluid dynamics model and an empirical model. Estimated standard errors in the flight test data are ±2.4% in lift coefficient, ±2.7% in drag coefficient. The flight test data also shows the aircraft to have a maximum lift to drag ratio of 10.5 at Mach 0.32, a zero lift drag coefficient of 0.0376 and an induced drag correction factor of 0.0607. When comparing the characteristics from the other models, the best overall comparison with the flight test data, in terms of lift coefficient, was with the empirical model. For the drag comparisons, all the models under predicted levels of drag by up to 43% when compared to the flight test data, with the best overall match between the flight test data and the 10% scale wind tunnel model. These discrepancies were attributed to various factors including zero lift drag Reynolds number effects, omission of a propeller system and surface excrescences on the models, as well as surface finish differences.

Keywords: Flight test, computational fluid dynamics, wind tunnel aerodynamics, empirical model

NOMENCLATURE

A	wing reference area (m^2)
b	aircraft span (m)
c	mean aerodynamic wing chord (m)
D	aircraft drag (N)
C_D	drag coefficient
C_L	lift coefficient
C_P	power coefficient
C_Q	torque coefficient
C_W	weight coefficient
c_f	skin friction coefficient
d	propeller diameter (m)
g	acceleration due to gravity (m/s^2)
J	advance ratio
K	induced drag correction factor
l	fuselage length (m)
L/D	Lift to drag ratio
Re	Reynolds number based on wing chord
V	aircraft velocity (m/s)
Q	engine torque (Nm)

q	dynamic pressure (Pa)
T	engine thrust (N)
y^+	non-dimensional wall distance
x-y-z	aircraft axes (m)
α	angle of attack (^{o})
ρ	air density (kg/m^3)
η	efficiency
ω	engine rotational speed (rads^{-1})
γ	flight path descent angle (^{o})

Subscripts

b	aircraft body
in	supplied to system
m	measured from instrument
prop	propeller

Acronyms

AR	wing aspect ratio
ARINC	Aeronautical Radio Incorporated
ADC	air data computer
CFD	computational fluid dynamics
CI	confidence interval
EAS	equivalent airspeed
ESDU	Engineering Sciences Data Unit
IRS	inertial reference system
ISA	international standard atmosphere
MAC	mean aerodynamic chord
NI	National Instruments
RPM	revolutions per minute
TAS	true airspeed
WT	wind tunnel

1. INTRODUCTION

In the field of full scale aircraft aerodynamics, many challenges still exist in predicting the aircraft performance, particularly at high Reynolds numbers and transonic Mach numbers [1,2]. More specifically, if modelling an aircraft in a wind tunnel, model scale and tunnel conditions generally result in one of the non-dimensional variables of interest being incorrectly scaled and methods such as boundary layer transition trips are required [3]. Numerical or computational fluid dynamic (CFD) modelling schemes of full scale aircraft have advanced substantially since the 1970's but assumptions must still be made. For example, if a complete solution of the Navier Stokes equations was to be obtained, a direct numerical simulation (DNS) would be required where the mesh density scales with Reynolds number $Re^{9/4}$ [4]. Therefore, given large civilian aircraft have Reynolds numbers based on wing chord in excess of 10 million, three dimensional mesh sizes in excess of 1 x 10^{15} cells would be needed for a DNS model. To address this mesh limitation, turbulence models and other advanced numerical schemes have led to significant developments in alternative numerical methods, based on the Reynolds Average Navier Stokes (RANS) equations and more recently Detached Eddy Simulation (DES) and Large Eddy Simulation (LES) methods [5,6]. However, there is still a need for numerical model validation through either flight test or wind tunnel testing.

In flight test it is possible to correctly scale both Mach and Reynolds number to measure an aerodynamic system of interest on a full scale aircraft [7,8]. This approach, however, has challenges in terms of finding a suitable flight test technique, but also in finding a suitable flight test platform, which can modified within an available budget and to the satisfaction of the certification authorities [9,10]. Furthermore, the flight test facility is likely to need specialist instrumentation [11,12].

The nature and associated costs of research flight testing has historically limited its use to national facilities, funded by organisations such as NASA, DLR or ONERA [13-16], or by large aerospace companies such as Airbus [17]. In all these cases, regular research campaigns using flight test platforms have allowed the study of challenging flow regimes such as laminar flow transition [18,19] and the development of complex aircraft systems [13,14]. These advantages and limitations of flight test, however, must also be considered against the advantages but also limitations of both numerical and wind tunnel test campaigns. For example, the increasingly complex numerical methods, although allowing detailed studies of the flow field, require increasing computational resources. In wind tunnel testing, the increasing demands of wind tunnel size and instrumentation for data fidelity, must also be balanced by the accuracy of the data required and the associated cost.

The objective of the following paper is to compare full scale lift and drag flight test data to other comparable models, including a numerical RANS CFD model, an empirical model based on Engineering Science Data Unit (ESDU) methods [20] and data taken from two wind tunnel models, One of the wind tunnel data sets is historical data from tests by the original equipment manufacturer (OEM), Handley Page Ltd [21]. The flight test data presented in this paper has been recorded from over 1000 flights and includes methods of data validation for both the drag and angle of attack. At the time of writing, the authors believe this amount of flight test data in combination with the thrust validation analysis, has not been published before, from an equivalent turboprop aircraft. Hence this data presents the aerodynamic community with valuable reference material for future modelling and validation. To this end, the basic surface model will be made publically available through the corresponding author who can be contacted directly. In the paper, from general comparisons of the different models with flight test, the authors discuss and explain the differences between the model data sets and the flight test data.

2. JETSTREAM 31 FLYING LABORATORY

The flying laboratory is a modified British Aerospace Jetstream 3102, twin turboprop aircraft. This commuter category aircraft has 19 passenger seats, with 18 of these seats in six rows of three. The aircraft was acquired by Cranfield University in 2002 and underwent a major modification to become a flight test laboratory.

The aircraft modification included the installation of seat back displays for each flight test observer and the fitting of new instrumentation, including a P.C., a National Instruments (NI) PCX data acquisition system, new sensors on the control surfaces and an ARINC connection from the Shadin 2000 cockpit air data computer (ADC) to the PC based acquisition rack. The seat back displays, by using Labview, can display live data of many aircraft systems or fitted sensors, as required for a particular test flight profile. Figure 1 shows a general schematic of the aircraft instrumentation and Figure 2 illustrates a typical Labview data acquisition screen used when acquiring aerodynamic data in flight.

2.1 Flight Test Technique

In a lift and drag flight test, at the time of the measurement, the aircraft weight is equated to the aircraft lift and the engine thrust is equated to aircraft drag. As the zero fuel mass of the aircraft (4980 kg), the fuel mass and the passenger mass is known at any point in the flight, the total mass of the aircraft and hence weight will equal the lift force. Errors in aircraft mass are shown in Table 1. Thus given the error in the lift coefficient C_L is primarily dependent on the mass error of

the aircraft, the air density error and the error in the true airspeed (TAS), given typical errors in TAS of ±2 knots, the errors in lift coefficient C_L are estimated to be ±2.4% of full scale.

The engine thrust is calculated from engine parameters as outlined in section 2.2. Validation of this method is described in section 2.3 and from this analysis, the error in drag coefficient C_D, is estimated to be ±2.7% of full scale.

Errors in angle of attack α are estimated to be a maximum of ±0.085º as outlined in section 2.4. A summary of the flight test errors are given in Table 1.

Variable	**Standard error**
Aircraft empty mass	±0.1%
Passenger mass	±0.7%
Fuel mass	±0.3%
ADC air density ρ (kg/m^3)	±0.8%
True airspeed TAS	±2 knots (±1.8% at 220 knots)
Lift coefficient C_L	±2.4%
Drag coefficient C_D	±2.7%
Angle of attack α (º)	±0.085º

Table 1 – Summary of estimated flight test errors (C_L, C_D as a % of full scale, mass % errors based on a total mass of 6900 kg, a passenger mass of 1400 kg and a fuel load of 500 kg, 7000 feet ISA)

For a lift and drag flight test, a set of straight and level conditions are flown through a range of equivalent airspeeds (EAS) to provide a consistent range of lift coefficients (C_L), drag coefficients (C_D) and body angle of attack (α_b) data. Body angle of attack, discussed in section 2.4, is used instead of the wing angle of attack (α) as the wing is twisted. The flight tests are generally performed between 5000 – 10000 feet altitude, based on an altimeter standard pressure setting (1013mbar) to allow the observers to also record a range of performance data. Stalling the aircraft is not permitted and therefore the data recorded is restricted to the linear portion of the C_L-α_b characteristic. For comparisons, historical lift and drag data from 1000 flight tests over the last 5 years are used to provide confidence intervals for comparison with the other models in this report, which include a CFD model, an empirical model and wind tunnel models. From the historic flight test data, the C_L- α_b curve in the linear region takes the form:

$$C_L = 0.3305 + 0.1052\alpha_b \quad (1)$$

where α_b is in degrees. The aircraft drag polar takes the form:

$$C_D = 0.0376 + 0.0607C_L^2 \quad (2)$$

which corresponds to a maximum lift to drag ratio of 10.5 at a maximum Mach number of 0.32. This Mach number also defines the upper limit of validity for the C_L- α_b characteristic and drag polar. Based on the C_L- α_b characteristic and the drag polar, at a flight test condition of 7000 feet

International Standard Atmosphere (ISA), Table 2 shows corresponding Equivalent Air Speed (EAS) conditions and the range of C_L-C_D-α_b values, Reynolds and Mach numbers obtained for an aircraft mass of 6900kg.

Equivalent Airspeed V_e (knots / m/s)	**Body Angle of Attack α_b (°)**	**Lift Coefficient C_L**	**Drag Coefficient C_D**	**Reynolds number Re (x10^6)**	**Mach number M**	**Lift to Drag Ratio**
210 / 108.0	0.45	0.378	0.04625	12.7	0.317	8.16
195 / 100.3	1.02	0.438	0.04924	11.8	0.295	8.89
175 / 90.0	2.03	0.544	0.05554	10.6	0.265	9.79
145 / 74.59	4.39	0.792	0.07566	8.77	0.219	10.5
130 / 66.87	6.22	0.985	0.09651	7.86	0.197	10.2
120 / 61.73	7.85	1.156	0.11874	7.26	0.181	9.74
112 / 57.61	9.48	1.327	0.14453	6.77	0.169	9.18

Table 2 – Flight test conditions at 7000 feet ISA based on drag polar data and an aircraft mass of 6900kg

2.2 Measurement of Aircraft Thrust

Calculation of in-flight drag assumes an equilibrium between engine thrust and aircraft drag in straight and level flight with the engine thrust corrected for the aircraft pitch attitude and horizontal flight path. However, in this set-up, engine thrust is not measured directly due to the restrictions in certification and modification of the aircraft powerplant. Instead the thrust is estimated from knowledge of the engine rpm and torque at a measured ambient and true airspeed and with reference to the manufacturer's data sheets of the propeller system. Thus, given torque coefficient C_Q is found from:

$$C_Q = \frac{Q}{\rho\omega^2 d^5} \tag{3}$$

where Q is the engine torque, ρ is the air density and d is the propeller diameter, the power coefficient C_P is found from:

$$C_P = 2\pi C_Q \tag{4}$$

Furthermore given the true airspeed V_{TAS}, if J is the propeller advance ratio which is found from:

$$J = \frac{V_{TAS}}{\omega d} \tag{5}$$

from a manufacturers lookup table, with values of C_P and J, the thrust coefficient C_T can be obtained. The propeller efficiency is then found from:

$$\eta_{prop} = \frac{1}{2\pi}\frac{C_T}{C_Q}J \quad (6)$$

which can finally be used to calculate engine thrust T where:

$$T = \frac{\eta_{prop} P_{in}}{V_{TAS}} \quad (7)$$

and where the power supplied to the propeller P_{in} is found from:

$$P_{in} = 2\pi\omega Q \quad (8)$$

This process is illustrated in the Figure 3.

Therefore to calculate the thrust in real time during the flight, the torque signal, rpm and ADC data is fed into the on-board PC through a NI PCX analogue to digital interface and Labview virtual instrument (VI) code. The Labview code then uses a series of look-up tables generated from the propeller datasheets to convert the torque, rpm and propeller characteristics into an estimated thrust. These values are displayed on a screen to the student engineers as shown in Figure 3.

2.3 Validation of Thrust Measurement

The estimation of engine thrust using the method outlined in section 2.2 requires a form of validation. In this paper we present a validation method which incorporates a known change in drag by reconfiguring the aircraft using the landing gear. This change in drag, calculated from the engine thrust, is then compared to published data. This method is a modification of the drift-down flight test technique, used to establish the one-engine-inoperative (OEI) ceiling for multi-engined aircraft.

Therefore, in this flight test method, the aircraft is initially trimmed at a convenient airspeed and altitude. Then, without touching the engine power lever, or throttle, the aircraft is zoom-climbed to an altitude at least 500 ft above datum. At this altitude, the undercarriage is deployed and the original airspeed quickly re-established. As the drag now exceeds the engine thrust, the aircraft will start to descend and a timed descent over 1000 ft (±500 ft from datum) can be conducted, once the rate of descent stabilises. If the pitch attitude is low, then in level flight thrust T equals drag D and lift W equals aircraft weight mg, i.e. T = D and L = W = mg. But in a steady descent at a flight path angle γ:

$$T = mg\sin\gamma = D + \Delta D \quad (9)$$

and

$$L = mg\cos\gamma \quad (10)$$

However, as the engine thrust is unchanged:

$$\Delta D = mg \sin\gamma \quad (11)$$

Converting into coefficient form by dividing with qS, where S is the reference area and the dynamic pressure $q = \frac{1}{2}\rho V_{TAS}^2$ leads to:

$$\Delta C_{D0} = \frac{2mg \sin\gamma}{\varrho V_{TAS}^2 S} = C_W \sin\gamma \quad (12)$$

where the weight coefficient $C_W = 2mg/\rho V_{TAS}^2 S$. Therefore using this methodology, it is possible to determine ΔC_{D0} if the test technique is repeated at a range of airspeeds, through the same altitude band. Hence since the value of flight test ΔC_{D0} relies on thrust calculated from the thrust estimate method (section 2.2), given the geometry of the undercarriage, the thrust can be implicitly validated by comparison of the flight test ΔC_{D0} with an empirical estimate of undercarriage ΔC_{D0} [22].

Based on this validation technique, Figure 4 shows a recent set of 37 flight test points gathered from the drift down method with the undercarriage deployed, resulting in a least squares fit relationship of $\gamma = 1.786 C_W^{-1.109}$. The 95% confidence interval with 37 points is γ = 0.61°, with a standard error of ±0.051° equivalent to ±1.6% of full scale and a coefficient of determination R^2 = 0.70. Hence if errors in C_W are included, from the flight test data in Figure 4, ΔC_{D0} = 0.0322±0.0009, i.e. a standard error of ±2.7%. To validate this magnitude of ΔC_{D0}, given dimensions of the undercarriage and by using the empirical method by ESDU [22], which has a stated accuracy of ±15%, in this case the undercarriage increment is ΔC_{D0} = 0.0355±0.0053. Thus within the accuracy of the method stated here, the thrust methodology in section 2.2 is assumed to be valid.

2.4 Measurement of Angle of Attack

The measurement of angle of attack is referenced with respect to the fuselage centreline and is termed body angle of attack (α_b). A wing chord line was not used as an α reference line as the wing is twisted from root to tip. Two sources of measuring α_b in flight are available on the aircraft which include an inertial reference system (IRS) unit in the back of the aircraft cabin and a calibrated external AoA vane, mounted on the starboard side of the nose. Due to the position of the nose vane and the potential position errors in α_b from this source [23], a series of flight tests were performed using a digital inclinometer to check both the outputs from the IRS and the calibrated nose AoA vane. The digital inclinometer, with a resolution of ±0.01°, based on the fuselage reference line, was mounted onto the airframe in the cockpit during the series of flight tests. The tests involved a similar set of straight and level lift and drag points to obtain a range of angles of attack, with sideslip angles estimated to be less than 2°. The results from these tests, relative to the fuselage centreline, are shown in Figure 5. In this case the standard error in α_b from the IRS is estimated to be ±0.085° and the standard error in α_b from the nose AoA vane is estimated to be ±0.064°. In both cases, the coefficients of determination R^2 were better than 0.97. The performance of the AoA vane with sideslip angles greater than 2° involve greater errors and are the subject of a separate, future publication.

3. COMPARISON MODELS

The following section describes the models used for comparison with the flight test data. These include a computational fluid dynamic (CFD) numerical model, a semi-empirical model and two wind tunnel models, one based on historical data published by the first manufacturer of the

Jetstream, Handley Page Ltd. The following shorthand labels will be used when presenting data in the remainder of the paper:

i) flight test data – Flight Test
ii) computational fluid dynamic numerical model – CFD
iii) empirical ESDU based model – Empirical
iv) Cranfield wind tunnel model – Cranfield WT
v) Handley Page wind tunnel model – HP WT

3.1 Computational Fluid Dynamic Numerical Model

For comparisons with the wind tunnel and flight test data, a computational fluid dynamics (CFD) model [24] was developed based on a previous solid model by Robert Parker [25]. The original geometry had minor differences when compared to the aircraft as summarised in Table 3. These differences also included modified wing and tailplane chord lengths, by inclusion of blunt trailing edges of thicknesses of less than 0.17% of mean aerodynamic chord. The resulting aspect ratio difference was less than 2% smaller than the real aircraft, which at peak lift to drag was expected to modify overall drag by less than 1% when compared to a CFD model with exact dimensions. These blunt trailing edges were used to aid the meshing process, while maintaining the basic aerofoil profiles. Any area differences between the real aircraft and CFD geometry were incorporated into scaling and coefficient calculations. The basic solid model is illustrated in Figure 6, where the trimmed wing trailing edge is also visible.

Aircraft Section	CATIA Model	Aircraft
Aircraft length (mm)	14.31	14.36
Wing span (mm)	15.83	15.85
Wing tip chord (mm)	0.830	0.790
Wing gross area (m^2)	25.60	25.08
Aspect Ratio	9.79	10.0
Tail span (mm)	6.61	6.60
Tail tip chord (mm)	0.653	0.686
Fin tip chord (mm)	0.844	0.889

Table 3 – Differences in geometry between aircraft and CFD model

The CFD model was based on a Reynolds Averaged Navier Stokes (RANS) solution without propellers on the aircraft. A hybrid mesh was developed using a mesh resolution study in Ansys ICEM CFD. For all the simulations, the aircraft was placed inside a cylindrical fluid domain with inlet and outlet dimensions of 10 times the aircraft fuselage length upstream and downstream and a far field with a radius of 5 fuselage lengths from the aircraft body. This allowed a pressure far field boundary condition to be set. Figure 7 illustrates the far field and aircraft surface mesh. Ansys Fluent 14.0 was used as a solver and coefficients of lift and drag were monitored with convergence criteria met when perturbations in lift and drag coefficient reached less than 1E-04 in both cases.

Several mesh densities were produced with respect to the turbulence model criteria and y+ requirements. Due to the computational resources and time available, meshes meeting the near wall turbulent model requirement of y+ = 1 – 5, although desirable in a future study, were not possible for this study. Therefore meshes were restricted to higher y+ values for use with a standard wall function [26]. Hence in the first stage of the mesh resolution study, two fine mesh

densities were produced with a y+ = 29 and y+ = 50 using a Spalart Almaras (SA) turbulence model with around 7.4M cells. Here the boundary layer region was meshed with prism cells up to y+ 1000 with an expansion ratio of 1.2 and tetra cells for the far field for a flight test condition equivalent to 195 knots EAS or 100.3 m/s. The results from this initial mesh resolution study are shown in Table 4. These initial results showed there was no significant change in the overall lift or drag characteristics. Therefore further stages of mesh resolution refinement were completed using y+ = 50 for the first prism cell.

In the second stage of mesh resolution refinement, the overall mesh density was changed from 7.4M cells down to 3.0M cells over 4 stages, with solutions again obtained for a SA turbulence model and the same flight test conditions. Table 5 summarises the solutions for the four different meshes and Figure 8 also shows the variation in lift and drag coefficient. The variation in lift and drag coefficients between the medium and fine mesh at the highest angle of attack of 9.4° is 0.76% and 0.25% respectively. Hence from these results and given the computational resources and the time available, the medium mesh with 5.6M cells was chosen for the final stage of mesh resolution refinement.

In final stage of mesh resolution refinement, a set of solutions was obtained using the medium mesh density with a number of different turbulence models. These models included the SA model, the k-ε model and k-ω SST models. Table 6 summaries the results of this study.

y+	C_L	ΔC_L (%)	C_D	ΔC_D (%)
50	0.46397	-	0.041440	-
30	0.46403	0.013	0.041698	0.62

Table 4 – Initial mesh resolution study with y+ 30 and y+ 50.

Mesh	Coarse	Intermediate	Medium	Fine
Initial prism height (mm)	0.2379	0.2379	0.2379	0.2379
Number of prism layers	9	10	10	10
Prism expansion ratio	1.25	1.23	1.2	1.2
Mean quality	0.794	0.799	0.808	0.822
Number of Cells (M)	3.0	4.6	5.4	7.4
C_L (α = 1.9°)	0.4619	0.4632	0.4640	0.4651
ΔC_L (%)	-	0.27	0.17	0.24
C_D (α = 1.9°)	0.04361	0.04072	0.04144	0.04041
ΔC_D (%)	-	-6.64	1.78	-2.49
C_L (α = 9.4°)	1.129	1.105	1.050	1.042
ΔC_L (%)	-	-2.20	-4.95	-0.72
C_D (α = 9.4°)	0.1670	0.1606	0.1593	0.1589
ΔC_D (%)	-	-3.84	-0.80	-0.25

Table 5 – Mesh densities developed

These results show, when compared to the flight test data, the best overall CFD model for both the low and high angles of attack and in terms of both the lift and drag predictions, was the SA model, with a minor improvement in lift prediction at higher angles of attack from the k-ε model. Therefore in the following comparisons, data will be presented from the CFD model using a medium mesh density and the SA turbulence model.

	SA model	k-ω SST model	k-ε model	Flight Test
C_L (α = 1.9°)	0.467	0.4401	0.4401	0.5304
ΔC_L (%)	12.0	17.0	17.0	
C_D (α = 1.9°)	0.04144	0.03948	0.03948	0.05468
ΔC_D (%)	24.2	27.8	27.8	
C_L (α = 9.4°)	1.032	0.9929	1.1328	1.319
ΔC_L (%)	21.8	24.7	14.1	
C_D (α = 9.4°)	0.09708	0.09418	0.1103	0.1433
ΔC_D (%)	32.3	34.3	23.0	

Table 6 – Summary of turbulence model summary using the medium mesh density

3.2 Empirical Model

In order to compare the flight test data and wind tunnel data with additional data including the CFD, the following briefly outlines an empirical model based on ESDU published methods for generic aerodynamic shapes. This approach uses look-up tables for each significant aerodynamic lift and drag component of the aeroplane including the wings, tailplane and fuselage. Given relevant geometric information on each component, look-up tables are generated using the corresponding empirical formulas based on parameters such as aspect ratio, chord, wing section, wetted area and flight conditions. For a given flight condition, simply interpolation is then used to output the overall aircraft lift and drag coefficients. This approach allows rapid prediction of the aircraft aerodynamic performance, without the computational overheads associated with RANS CFD methods and is suitable for adaption in a standard spreadsheet such as Excel. Full details of the model are outlined in the report by Cooke [20].

3.3 Wind Tunnel Model

The Cranfield Jetstream 31 wind tunnel model is a 10% scale wooden model fitted with boundary layer transition strips on the wing and tailplane leading edges. Fuselage nose and mounting points on the underside of the wing are also fitted. The Cranfield model mounting points allow mounting at the 35% chord point, in an inverted position from the bottom of the wings in order to reduce interference effects. A rear sting is also fitted onto the model which, in conjunction with the use of the wing mounting points, allows the pitch and sideslip to be set with sideslip and angles of attack of up to 20°. The model was manufactured as part of a previous research project [25] to develop laser scanning techniques for solid models and as such has a black, smooth, shiny surface finish throughout. The model also includes elevator, rudder and flap control surfaces to allow configuration changes representative of the real aircraft. Furthermore, the addition of different engine nacelles is possible to allow the simulation of a Jetstream Mark 1. In these measurements, however, the model has been fitted with Honeywell TPE331 engine nacelle profiles as found on Jetstream 31 and 32 aircraft, which is the full sized flight test aircraft. Figure 9 illustrates the Jetstream model mounted in the wind tunnel working section.

Additional data from Handley Page, outlined in the wind tunnel report by Storey [21], was also available for comparison with the flight test data. The Handley Page wind tunnel model included minor differences which are summarised in Table 7. Both models did not include propellers or a propulsion system and the CFD model was set-up to reflect this configuration.

	Cranfield Model	Handley Page Model
Model Scale	10%	17%
Maximum Reynolds Number (Re)	0.488×10^6	1.2×10^6
Boundary layer transition position	5% MAC	5% MAC
Model section transitioned	wings, tail	nose, nacelle, tail
Tailplane angle relative to datum axes	0^o	0.45^o
Tailplane size	to scale	10% greater span

Table 7 – Summary of differences between the Cranfield and Handley Page wind tunnel models

Wind tunnel measurements were taken from the Cranfield 2.44m x 1.83m closed return, low speed wind tunnel. The tunnel has a maximum speed of 50m/s, but in practice is limited to 45m/s in sustained operation due to motor restrictions. Turbulence levels are better than 0.1%, The tunnel is also fitted with a six axis force balance with a full scale resolution in lift and drag of ±1.0N, ±0.9N respectively. This corresponds to a measured full scale resolution of ±0.47% in lift coefficient and ±1.6% in drag coefficient.

To complete the tare correction for the wind tunnel force balance, data was acquired for the model support structure with a T arrangement of 16mm diameter bars. Actual force measurements of the cross bar were taken but the longitudinal bar forces and moments were estimated using ESDU 80025 [27]. Further blockage and streamline curvature corrections were also applied to the data as outlined in the methodology by Barlow et al [3].

Wind tunnel tests were conducted at a nominal velocity of 40 m/s which corresponds to a model Reynolds number of 0.43×10^6 based on mean aerodynamic chord. This compares to a flight test Reynolds number of 8.2×10^6 which therefore required use of boundary layer transition strips for the wind tunnel measurements. The transition strips were 0.5mm and 0.25mm diameter wires located at 5% of model mean aerodynamic chord on the wing and tailplane sections respectively. The model was also tested in a clean configuration (no flap) at different angles of attack (-5° to 15°) airspeeds (30 m/s to 45 m/s) and sideslip angles (0° to -20°). The matrix of test points is shown in the Table 8, where the model was measured using a pitch and hold technique with 1^o angle of attack increments.

Wind tunnel Speed (m/s)	Reynolds No ($\times 10^6$)	Angle of Attack (^{o})	Sideslip Angle (^{o})
30	0.326	-5^o to $+15^o$	0^o
35	0.380	-5^o to $+15^o$	0^o
40	0.434	-5^o to $+15^o$	0^o to -20^o
45	0.488	-5^o to $+15^o$	0^o

Table 8 – Wind tunnel measurement conditions

4. RESULTS AND DISCUSSION

In the following, the flight test data is compared to results from the CFD model, the wind tunnel testing including selected Handley Page results [21] and the empirical model. The comparisons are in three parts including the lift characteristics, the drag polar and specific examination of the drag components of the aircraft. The discrepancies and possible improvements to the different datasets will also be discussed.

4.1 Lift-curve slope comparisons

Figure 10 shows the C_L-α_b flight test data based on over 1000 datapoints taken over a 5 year period of testing. In this case, α_b is in degrees and is based on the body reference line. Regression analysis of the data has an R^2 of 0.97 with a function $C_L = 0.3305 + 0.1052\alpha_b$ and a 95% confidence interval of ±0.09C_L. If the empirical model is compared to the flight test data, as shown in Figure 11, the empirical lift-curve slope is predicted to be $C_L = 0.338 + 0.1099\alpha_b$. which lies within the 95% confidence level of the flight test data. Further comparisons of the CFD, Cranfield WT and Handley Page WT with the flight test data are also shown in Figure 11 and summarised in Table 9. If the overall characteristics are considered with respect to the flight test data, the empirical model is the closest prediction to the flight test data followed by the CFD model and then the Handley Page WT data. The poorest C_L-α_b comparison with the flight test data is the Cranfield WT data.

It should be noted that the stall angle α_{stall} and C_{Lmax} cannot be predicted from the empirical model or the CFD model. In the first case, this is because the functions available to generate the look up tables for the empirical model are based on the linear portion of the C_L-α data. For the CFD model, a steady-state RANS solution will not predict what is an unsteady flow phenomena, found in the stall region. Therefore steady-state RANS predictions of stall, α_{stall} and C_{Lmax} are not to be considered reliable.

Data set	a_o (C_L)	a (C_L / °)	C_{Lmax}	α_{stall} (°)	Comments
Flight test	0.3305	0.1052	-	-	Datum data
Empirical	0.3380	0.1099	-	-	Closest prediction of C_L to flight test data.
CFD	0.2928	0.0937	-	-	Under-predicts C_L, within C.I. of flight test data. Discrepancies due lack of propellers and y+ levels
HP WT	0.1704	0.1003	1.28	16.5	Under-predicts C_L, outside C.I. of flight test data. Lack of propellers and Re related effects.
Cranfield WT	0.1489	0.0765	0.99	14.0	Under-predicts C_L, outside C.I. with greatest deviation from flight test. Lack of propellers, also lowest Re of all models

Table 9 – Comparison of linear lift curve slope characteristics and other C_L-α data (based on the linear portions of the lift-curve slopes with R^2 = 0.99 for all cases)

The C_L-α_b discrepancies of the models with the flight test data can be attributed to a number of effects including wind tunnel Reynolds number effects and the fidelity of the wind tunnel and CFD models which do not include propeller effects. These discrepancies will now be discussed in more detail.

Considering the wind tunnel data, given this data has been corrected for tare, blockage and streamline effects, the remaining significant uncorrected effect is for Reynolds number. In this

case, the Handley Page data has the closest Reynolds number to the flight test at 1.2 x 10^6 compared to the Cranfield wind tunnel data with 0.434 x 10^6. The flight test Reynolds numbers vary between 6.8 x 10^6 – 12.7 x 10^6. The Cranfield wind tunnel data also included tests over Reynolds number ranges of 0.326 x 10^6 to 0.488 x 10^6. In both cases and when taking into account experimental error, the Handley Page and Cranfield data did not indicate any significant change of the C_L-α_b curve over these Reynolds number ranges.

Examining the literature on Reynolds number corrections, NACA data [28] and ESDU analysis [29] indicates part of the discrepancy between wind tunnel and flight test can be accounted for by correcting the wind tunnel data with an additional factor based on Reynolds number. In this case there is a Reynolds number factor of 3 – 10 times for the Handley page data and 15 – 30 times for the Cranfield data compared to flight test. Examining simple 2D aerofoil data from NACA [28], significant increases in C_{Lmax} of up to $\Delta C_L = 0.4$ are possible with these Reynolds number factors for the majority of aerofoil sections at these Mach numbers. Even with a correction for aspect ratio [30], this C_L increase is still expected to be around 70 – 80% of this value, i.e. a maximum $\Delta C_L = 0.3$. There is also expected to be a change in lift-curve slope due to Reynolds number as suggested by ESDU [29], NACA [28] and previous reviews [31]. In this case, an increase of up to 10% in the CL-α slope is possible, but this factor is highly sensitive to the shape of the aerofoil and the whether a transition strip is present or not [28]. Therefore the inclusion of the transition strips on the Cranfield wind tunnel model is likely to have a Reynolds correction effect which explains the different C_L-α slope. But it is not possible to precisely account for the proportion of this correction on the C_L-α data. The Handley Page data [21] is further complicated by the limited use of boundary layer transition strips (nose, nacelle, tail only), although flow visualization data in the Handley Page report suggested transition on the wings at $\alpha_b = 0^o$ of around 65% – 75% MAC [21].

For the wind tunnel data, a further effect, which is known to occur in the presence of a propeller, is augmented lift over the section of the wing, affected by the propeller slipstream [32-34]. As with boundary layer transition strips, the augmentation in terms of C_L is highly configuration dependent, but at angles of attack of 10^o would be expected to generate between 10% – 20% higher levels of C_L than an un-augmented wing. As both wind tunnel models did not include propellers, this omission in the models will contribute to the under-prediction of C_L compared to flight test.

For comparison of the CFD data to flight test, although the CFD has correctly scaled Reynolds numbers, the boundary layer is unlikely to match the flight test as the y+ values have been restricted to between 30 – 50 and rely on a standard wall function [26]. Also as with the wind tunnel data, the CFD data has no propeller effects. Therefore it would be expected to have a lower lift coefficient than the flight test data, but a higher C_L than the wind tunnel data, which can be clearly seen in Figure 9. Here the CFD data lies within the 95% confidence interval of the flight test data, but there is a slight under-prediction in C_L of around $\Delta C_L = 0.1$ in the linear portion of the C_L-α curve. Addition of a propeller user defined function to the CFD model should reduce this discrepancy and increase the C_L prediction in the CFD. At the time of writing, this CFD model refinement is ongoing and will be the subject of a further paper.

4.2 Drag polar comparisons

The following will present the drag characteristics of the flight test data, with comparisons to the wind tunnel data, including the Handley Page model, the CFD data and the empirical model prediction. Discrepancies in drag will be highlighted and accounted for where possible, based on ESDU and other published material.

Initially if we examine the flight test drag data, Figure 12 illustrates the C_L^2 vs. C_D characteristic with a best fit line obtained from regression analysis yielding the characteristic $C_D = 0.0376 + 0.0607C_L^2$ with a maximum lift to drag of 10.5 at a peak Mach number of 0.32 and a zero lift drag of $C_{D0} = 0.0376$. The data has a 95% confidence level of $\Delta C_{D0} = 0.0021$ and a $R^2 = 0.98$.

Figure 13 shows the flight test data plotted with the wind tunnel data, the CFD model and the empirical model predictions. If the most linear portion of the C_L^2 vs. C_D characteristic adjacent to the flight test data is also analysed using linear regression, Table 10 shows the equivalent C_L^2 vs.

C_D characteristics from the other data sources. This summary table shows that in terms of the overall performance from $(L/D)_{max}$, the Cranfield wind tunnel data gives the best overall match to the flight test data. This is confirmed in Figure 13 where the wind tunnel data in this case closely matches the flight test data in the most linear portion of the characteristic. The next closest overall comparison is the CFD prediction followed by the Handley Page wind tunnel data, with the greatest overall C_D discrepancy between the flight test data and the empirical model.

Data	C_{D0}	K	$(L/D)_{max}$	R^2	Comments
Flight test	0.0376	0.0607	10.5	0.98	Datum data
Cranfield WT	0.0508	0.0307	12.7	0.97	Closest L/D match and C_D match up to C_L = 0.9. Re effects on C_{Do} contribute to over-prediction
CFD	0.0285	0.0522	13.0	0.98	Under-prediction of drag related to limitations of turbulence model and y+ levels
HP WT	0.0234	0.0516	14.4	0.98	Under-prediction of drag related to Re effects and boundary layer transition configuration
Empirical model	0.0202	0.0326	19.5	-	Over-simplified treatment of geometry and zero lift drag sources result in greatest under-prediction of drag

Table 10 – Comparison of linear C_L^2-C_D characteristics from the different data sources

4.2.1 Wind tunnel vs. flight test

Examining the wind tunnel characteristics with the flight test in more detail, shows the Cranfield wind tunnel zero-lift drag coefficient C_{D0} is 35% higher than the flight test data. The corresponding value of induced drag correction factor K for the Cranfield wind tunnel is also nearly half the magnitude of the flight test value. If we initially consider C_{D0}, this over-prediction in drag coefficient is likely, in-part, to be related to the lower Reynolds numbers of the wind tunnel data. For example, based on flat plate turbulent boundary layer characteristics, skin friction coefficient would be 70% higher at the wind tunnel Reynolds number of 0.434 x 10^6 compared to the flight test Reynolds number of 6.8 x 10^6. Thus with the transition strips on the leading edges of the Cranfield wind tunnel model, from this simple analysis, it would appear the strips reduce this discrepancy but they do not entirely correct the zero lift drag coefficient. The Reynolds number comparisons, over the tunnel speeds tested, within experimental error also did not account for the remaining discrepancy.

This type of Reynolds related effect is further reinforced if the Handley Page C_{D0} value is also examined. Here, the Handley Page wind tunnel C_{D0} is 38% lower than the flight test data. In this case though, the Handley Page model did not have transition strips and had observed transition on the wings at α_b = 0° of around 65% – 75% MAC. Using similar boundary layer analysis, an equivalent flat plate C_{D0} at the Handley Page Reynolds number compared to a fully turbulent value at Reynolds flight number gives an effective ΔC_{D0} difference of 5% (C_{Do} = 0.00305 with transition at Re = 0.5 x 10^6 and a Re = 1.2 x 10^6 compared with C_{Do} = 0.00318 for a fully turbulent with Re = 6.8 x 10^6). Therefore given boundary layer transition can be highly geometry specific, although simple Reynolds and boundary layer comparisons account in-part for this discrepancy, greater experimental detail on the local flow characteristics on the wind tunnel model are needed to clarify these different drag contributions.

It should also be noted that the both wind tunnel models did not include any propellers and as will be discussed in the next section, the effect of the propeller is expected to increase the drag coefficients on any wind tunnel model, although implementation of a correctly scaled propeller model in a wind tunnel is a highly challenging area [3].

4.2.2 CFD vs. flight test and propeller effects

If we now compare the CFD data with the flight test data, there is a clear under prediction in CFD drag coefficient from the overall trend and in the level of C_{D0}. This under prediction falls outside the 95% confidence interval of the flight test data for the majority of the CFD characteristic. In this case, the Reynolds numbers of the CFD were matched to the flight test conditions with the assumption of a fully turbulent flow over the aircraft. Therefore the discrepancy in drag coefficient is likely to be attributable to the performance of the turbulence model related to the y+ limitation and the standard wall function and other unaccounted sources of drag, such as the effects of the propeller slipstream, surface excrescences, external surfaces such as aerials and other surface deviations, including wheel bay cavities.

In the first case, the difficulties of estimating different components of drag in CFD methods are well known [35]. For example over the period of five AIAA drag prediction workshops (DPW1 to DP5) [35], the overall drag levels predicted from a wing body model have been refined by around 150 drag counts (ΔC_{D0} = 0.0150), although this process has involved increasing mesh sizes from 3 million to as high as 190 million cells where y+ = 1 were achieved. The DPW's have also assessed a wide range of turbulence models, which have included the turbulence models tested in this application. However, the resources available for this project prohibit the use of such large mesh sizes and therefore it must be concluded, part of the drag discrepancy is likely to be caused by the mesh limitations and turbulence model and wall function limitations of the CFD model.

Of greater significance is likely to be the exclusion of propeller effects in the CFD model, which did not include any propellers. Basic drag analysis of propeller systems [36-39] relates the drag generation to the slipstream effect of the propeller. This drag effect can be broken down into a parasitic component from local skin friction increases and an induced drag component due to the lift augmentation effect of the slipstream. If we apply a simple equivalent analysis [36] to the case of the Jetstream 31, the local parasitic component increase ΔC_{D0p} can be estimated from:

$$\Delta C_{D0p} = C_{D0l} \frac{S_I}{S_{wet}} \left[\left(\frac{V_s}{V} \right)^2 - 1 \right] \tag{13}$$

where C_{D0l} is the local skin friction coefficient, S_I is the area of the wing immersed by the slipstream, S_{wet} is the wetted area of the wing, V_s is the local slipstream velocity and V is the aircraft velocity. Therefore with propeller diameters of 2.69m at the mean aerodynamic chord of 1.86m, with S_{wet} = 41.88m^2, the ratio of slipstream area to wetted wing area is approximately 0.48. If we now consider the local change in dynamic pressure due to the increase in slipstream velocity ΔV_s, at the optimum flight test condition of $(L/D)_{max}$ = 10.5 at a true airspeed of V = 78 m/s at 7000 feet ISA, with a typical aircraft mass of 6900 kg, the thrust from each propeller is estimated to be T = 3220 N. Assuming an ISA density of ρ = 0.993 kg/m^3 and a propeller area of A = 5.68m^2, the slipstream velocity increment ΔV_s can be estimated using:

$$\Delta V_s = \frac{T}{\rho A V} \tag{14}$$

giving ΔV_s = 7.3 m/s which is equivalent to around a 20% increase in local dynamic pressure. Therefore if at these flight conditions we take the local turbulence skin friction coefficient of C_f = 0.0031, for a wing section with a form factor of 1.3, the local zero lift drag coefficient estimate is taken as C_{D0l} = 2 x 1.3 x 0.0031 = 0.00806. Using this local C_{D0l}, from equation (13) the local ΔC_{D0p} from the propeller slipstream effect is estimated to be ΔC_{D0p} = 0.00806 x 0.48 x 0.2 = 0.00077 or an increase of 2.7% in zero lift drag w.r.t. the CFD prediction of C_{D0}. At non-optimal (L/D) flight conditions which range from V = 62 m/s to V = 117 m/s, using similar analysis ΔV_s are estimated to be ΔV_s = 11.5 m/s and ΔV_s = 6.1 m/s with ΔC_{D0p} =0.0016 and ΔC_{D0p} =0.000385 respectively, corresponding to increases in C_{Do} of 5.6% and 1.4%. Therefore this simplified analysis indicates a minor dependency of C_{D0} on the aircraft flight speed. If corrected for this source of drag, the CFD C_{D0} at low airspeeds would still not lie within the confidence interval of the flight test data.

If the lift induced slipstream drag is now considered, adapting the analysis outlined in [36,37], the induced drag coefficient increase ΔC_{Di} from the propeller slipstream can be approximated to:

$$\Delta C_{Di} = \frac{\Delta C_L C_{L0}}{\pi AR} \quad (15)$$

where ΔC_L for n propellers is estimated from:

$$\Delta C_L = 0.5 \frac{TC_{L0}}{qA} n \left(\frac{d}{b}\right) \quad (16)$$

given the lift coefficient at a given flight speed without the propeller is C_{L0}, the dynamic pressure is *q*, the wing span is *b*, the propeller diameter is *d* and the wing aspect ratio is AR.
Therefore given optimum flight conditions as before at $(L/D)_{max}$, if C_{L0} = 0.8, q = 3020 Pa, with b = 15.85m, ΔC_L = 0.025. Therefore with AR = 10, ΔC_{Di} = 0.00064 which if the parasitic drag is now included, results in a total ΔC_D increase at this flight condition of ΔC_D = 0.00141 which is a 5% increase in C_{D0} above the current CFD prediction. As in the parasitic analysis, if we also consider ΔC_{Di} at flight conditions of V = 62 m/s to V = 117 m/s, with C_{L0} = 1.3 and 0.56 respectively, ΔC_L = 0.075 and ΔC_L = 0.01. These lift increments give corresponding induced drag increases of ΔC_{Di} = 0.0031 and ΔC_{Di} = 0.00018. Therefore the total ΔC_D increase at V = 62 m/s is ΔC_D = 0.0047 reducing at V = 117 m/s to ΔC_D = 0.00057. These total drag increases correspond to 16% and 2% of the current predicted CFD C_{D0}. Therefore at the lower flight speeds, the effect of the propeller slipstream is significant and would be expected to shift the CFD drag prediction into the 95% confidence interval of the flight test data. At higher flight speeds, however, the propeller effect on the drag coefficient is less significant and other sources of drag are therefore expected to contribute to the CFD drag discrepancy when compared to the flight test data.

4.2.3 Empirical model vs. flight test data

If we compare the empirical model characteristics to the flight test data, the prediction of zero lift drag C_{D0} is the lowest of all the measured or predicted values and is under-predicted by 43% compared the flight test data. This limitation of drag prediction is in contrast to the lift coefficient prediction of the empirical model (see Figure 11), which closely matches the flight test characteristic. However, the complex dependence of the different sources of drag to the pressure field generated by the body geometry is clearly difficult to capture using this type of simplified model. Also only gross dimensions and features are used in this model which over-simplifies all the different sources of zero-lift drag and results in an overall, significant under-prediction of drag. Stall behaviour also cannot be predicted. Part of this drag discrepancy may be corrected by the introduction of further factors into the model, but for a given aircraft shape, detailed knowledge is generally needed to ensure the correct range of factors are applied. The major advantage though with this type of model, is the rapid prediction possible using a macro-driven spreadsheet, which makes this method suitable for initial design predictions of an aircraft, or design refinement once the model is validated.

4.2.4 Other sources of drag

Examining both the wind tunnel model in Figure 9 and the CFD model in Figure 7, it can be seen that features such as aerials and other surface excrescences such as door handles, covers, ducts and other cavities have been omitted. It may be possible to include these features in both the wind tunnel and CFD models, but in many cases due to the scale or size of the features, it is not practical to implement them and in the case of the CFD model, the limitations of the mesh size also limits inclusion of these features. Therefore alternative methods of estimating these sources of drag need to be considered and then added to the total drag prediction of the aircraft. The simplest method is generally found in conceptual aircraft design methods such as outlined by Raymer [40]. In this case, Raymer recommends adding 10% to the zero lift drag to account for all of these drag sources. For the CFD prediction this would equate to ΔC_{D0} = 0.00285. Alternative methods are outlined by ESDU [41] and cover a significant range of excrescence items. In each case, inclusion of this source of drag and the effects of the propeller slipstream discussed

previously would move all the CFD drag prediction into the 95% confidence interval. The Handley Page prediction would also lie significantly closer to the flight test data.
A further source of drag which is omitted on the wind tunnel and CFD models originates from the elevator deflection required to trim the aircraft in steady flight. As Figure 14 shows, this deflection also depends on the centre of gravity (CoG) of the aircraft and can range from around 0.5º to 5º in the most forward CoG condition. From elevator data as outlined by Cooke [20], these elevator positions equate to drag increments predictions of ΔC_{D0} = 0.00026 at 0.5º to ΔC_{D0} = 0.0026 at 5º which ranges from an increase of 1% to 9% of the CFD predicted C_{D0}.
Finally surface finish is known to have an effect on the level of zero lift drag C_{D0} through increases in skin friction coefficient C_f [42,43]. Published data indicates dependence of C_f on Reynolds number, Mach number and surface roughness. Assessments by ESDU [43] of typical surface deterioration of an aircraft indicate increases in C_f of around 20% above smooth levels at the Mach numbers flown by the Jetstream. Although the aircraft surfaces are periodically cleaned, on average the surface cleanliness and finish of the actual aircraft would expect to result in higher levels of skin friction than the wind tunnel and CFD models. As with the other drag sources discussed previously, if these drag increments are also added to these predictions, further convergence of the CFD and wind tunnel results towards the flight test data would occur.

5. CONCLUSIONS

This paper has presented flight test data taken from the National Flying Laboratory Centre, Jetstream 31 twin turboprop aircraft. The aircraft is a commuter category aircraft with 19 seats and has been set up to demonstrate flight test techniques to aerospace engineers. Over the period of 10 years of operating the aircraft, over 1000 lift-drag data points have been analysed. The data presented here has allowed analysis of the basic lift and drag aerodynamic characteristics of the aircraft, with estimated standard errors of ±2.4% in lift coefficient and ±2.7% in drag coefficient. From recent flight tests, a drift-down technique has been used to validate the engine thrust and the standard error in angle of attack (AoA) was also estimated to be ±0.085º, if sideslip angles are limited to less than 2º in straight and level flight.

The paper has compared the flight test data to a steady state RANS computational fluid dynamic (CFD) model and two sets of wind tunnel data taken from a 10% and 17% scale model. All three models did not include propeller effects. Overall the CFD model gave the best lift characteristics with the majority of predicted points lying within the 95% confidence interval of the flight test data. The 10% scale wind tunnel model gave the best overall drag characteristics between lift coefficients of 0.5 – 0.9 with these data also lying within the 95% confidence interval of the flight test data. Further analysis of the effects of the propellers indicated inclusion of both the lift and drag increments, produced by the propeller slipstreams, would further shift points from the wind tunnel measurements and CFD predictions into the flight test confidence interval. The CFD mesh was also limited to y+ 30 – 50 causing a reduction in model fidelity. Further discrepancies in drag were thought to be attributable to the omission of features such as aerials and other excrescences on the CFD and wind tunnel models and differences such as surface finish and trim drag effects present in the flight test data.

A further comparison to the flight test data was also made using an empirical model based on ESDU methods. Although the empirical model could not predict the effects of stall, in terms of lift coefficient, the lift curve slope characteristic matched the flight test data to within 4.5%. However, the drag characteristic had a significant discrepancy both in terms of the zero lift drag and lift induced drag. This was attributed to simplifications made by the empirical model in terms of geometry, sources of zero lift drag and aerodynamic interactions between the fuselage and the wing.

ACKNOWLEDGEMENTS

The authors would like to acknowledge the staff of the Applied Aerodynamics wind tunnel workshops for their support in this work.

REFERENCES

1. Lan C.-T.E., Roskam J., “Airplane Aerodynamics and Performance” DARcorporation, Kansas, U.S.A. (2003)
2. Jameson A., Ou K., “50 Years of Transonic Aircraft Design”, Progress in Aerospace Sciences 47(5), p308-318 (2011)
3. Barlow J.B., Rae JR. W.H., Pope A., “Low-Speed Wind Tunnel Testing” Third Edition, Wiley, New York, ISBN 978-81-265-2568-3 (1999)
4. Gharib M., “Perspective: the experimentalist and the problem of turbulence in the age of supercomputers” *Journal of Fluids Engineering*, 1996, 118, 233-242
5. Spalart P.R. “Topics in Detached-Eddy Simulation”, Computational Fluid Dynamics 2004, Eds. Groth C., Zingg D.W., Proceedings of the Third International Conference on Computational Fluid Dynamics, ICCFD3, Toronto, 12–16 July 2004, p3-12 (2004)
6. Galperin B., Orszag S.A., “Large Eddy Simulation of Complex Engineering and Geophysical Flows” Cambridge University Press, Cambridge, U.K. (2010)
7. Stinton D., “Flying Qualities and Flight Testing of the Aeroplane” Blackwell Science Oxford, ISBN 0-632-05056-X (1996)
8. Ward D.T., Strganac T.W., “Introduction to Flight Test Engineering” Second Edition, Kendall/Hunt Publishing Dubuque, Iowa, ISBN 978-0-7575-3871-1 (2001)
9. “Advanced In-Flight Measurement Techniques”, Eds. Boden F., Lawson N., Jentink H.W. and Kompenhans J., Springer-Verlag Berlin Heidelberg ISBN 978-3-642-34737-5, p331-340 (2013)
10. Gratton G., “Initial Airworthiness – Determining the Acceptability of New Airborne Systems”, Springer International Publishing, ISBN 978-3-319-11408-8 (2015)
11. Burner A.W., Lokos W.A., Barrows D.A., “Aeroelastic Deformation: Adaptation of Wind Tunnel Measurement Concepts to Full-Scale Vehicle Flight Testing” NASA Langley, NASA Report TM-2005-213790 (2005)
12. Boden F., Jentink H., Petit C., “IPCT Wing Deformation Measurements on a Large Transport Aircraft” , Advanced In-Flight Measurement Techniques, Eds. Boden F., Lawson N., Jentink H.W. and Kompenhans J., Springer-Verlag Berlin Heidelberg ISBN 978-3-642-34737-5, p331-340 (2013)
13. Wallace L.E., “Airborne Trailblazer: Two Decades With NASA Langley's 737 Flying Laboratory”, Langley Research Centre, U.S. Government Printing Office, NASA SP-4216 (1994)
14. Wusk M., “ARIES: NASA Langley's Airborne Research Facility”, AIAA Paper 2002-5822, AIAA's Aircraft Technology, Integration, & Operations (ATIO) 2002 Technical Forum, 1 – 3 October 2002, Los Angeles, California (2002)
15. Baumgartner S.V., Rosigkeit D., Nottensteiner A., “Usability of LTE for Transmitting Radar Data from DLR’s Research Aircraft DO 228-212” Proceedings of the 36th European Telemetry and Test Conference, 10 – 12 May 2016, Nuremberg, Germany, ISBN 978-3-9816876-2-0, p181-187 (2016)
16. Maestrati J., Bulgubure Ch., *Laminar Flow for Business Jets : Falcon 900 HLFC Demonstrator*, 2nd European Forum on Laminar Flow Technology, Bordeaux, France, June, 1996
17. Reneaux J., “Overview On Drag Reduction Technologies For Civil Transport Aircraft” European Congress on Computational Methods in Applied Sciences and Engineering, ECCOMAS 2004, Neittaanmäki P., Rossi T., Korotov S., Oñate E., Périaux J., and Knörzer D. (eds.), Jyväskylä, 24—28 July 2004, p1 – 18 (2004)
18. Lee C.C., Obara C.J., Wusk M.S., “Flight-Measured Streamwise Disturbance Instabilities in Laminar Flow” AIAA Paper 90-1283-CP, Orbital Debris Conference: Technical Issues and Future Directions, April 16 – 19 1990, Baltimore, MD (1990)
19. Patzold A., Peltzer I., Nitsche W., “Sensors and Actuators for Laminar Flow Flight Experiments” , Advanced In-Flight Measurement Techniques, Eds. Boden F., Lawson N., Jentink H.W. and Kompenhans J., Springer-Verlag Berlin Heidelberg ISBN 978-3-642-34737-5, p331-340 (2013)

20. Cooke A.K., “A Simulation Model of the NFLC Jetstream 31” College of Aeronautics Report No. 0402, Cranfield University (2006)
21. Storey R.F.R., “H.P.137: Longitudinal and lateral static stability measurements on a 1/6th scale model” Wind Tunnel Report 3021, September 1966 (1966)
22. ESDU. “Undercarriage drag prediction methods”, *ESDU 79015*, 1987.
23. Lawford J. A. and Nippress K. R., Calibration of air-data systems and flow direction sensors. Advisory Group for Aerospace Research and Development (AGARD) Flight Test Techniques Series, 1(AG-300), 1984
24. Anderson JR. J.D., “Computational Fluid Dynamics: The Basics with Applications” McGraw-Hill Inc., New York, ISBN 0-07-001685-2 (1995)
25. Parker R., “Investigation and Development of a 3D Non-Contact Scanning Process for CFD Model Generation” PhD Thesis Cranfield University (2006)
26. Launder B.E. Spalding D.B. "The Numerical Computation of Turbulent Flows". Computer Methods in Applied Mechanics and Engineering. 3. 269–289. 1974.
27. ESDU 80025. Mean forces, pressures and flow field velocities for circular cylindrical structures: single cylinder with two-dimensional flow. ESDU International. June 1986
28. Jacobs E.N. and Sherman A., “Aerofoil Section Characteristics as Affected by Variations of the Reynolds Number’, NACA TR-586 (1937)
29. ESDU 05022. Extrapolating wind-tunnel data to full-scale Reynolds number Part 1: Principles. ESDU International. January 2006
30. Laitone E.V., “Lift-Curve Slope for Finite-Aspect-Ratio Wings”, Journal of Aircraft 26(8) p789-790 (1989)
31. Pate S.R., “Effects of Wind Tunnel Disturbances on Boundary-Layer Transition with Emphasis on Radiated Noise: A Review”, 11th Aerodynamics Testing Conference, Colorado Springs, Colorado, 18-20, 1980, AIAA Paper 80-0431 (1980)
32. Brenckmann M.E., “Experimental Investigation of the Aerodynamics of a Wing in a Slipstream”, Journal of the Aeronautical Sciences 25(5), p324 – 328 (1958)
33. ESDU 88031. Lift and longitudinal forces on propeller/nacelle/wing/flap systems. ESDU International. November 2009
34. Fink M.P., Mitchell R.G., White L.C., “Aerodynamic Data on a Large Semispan Tilting Wing With 0.5-Diameter Chord, Double-Slotted Flap, and Both Left- and Right-Hand Rotation of a Single Propeller” NASA TN D-3375, pp122 (1966)
35. David W. Levy, Kelly R. Laflin, Edward N. Tinoco, John C. Vassberg, Mori Mani, Ben Rider, Christopher L. Rumsey, Richard A. Wahls, Joseph H. Morrison, Olaf P. Brodersen, Simone Crippa, Dimitri J. Mavriplis, Mitsuhiro Murayama, Summary of Data from the Fifth Computational Fluid Dynamics Drag Prediction Workshop, Journal of Aircraft, 2014, Vol.51: 1194-1213, 10.2514/1.C032389
36. Biber K., “Estimating Propeller Slipstream Drag on Airplane Performance”, Journal of Aircraft 48(6) 2011 p2172 – 2174 (2011)
37. Hoerner, S. F., “Fluid-Dynamic Drag”, Hoerner Fluid Dynamics, Brick Town, NJ, 14.14-14.15 (1965)
38. Rakshith B.R., Deshpande S.M., Narasimha R., “Optimal Low-Drag Wing Planforms for Tractor-Configuration Propeller-Driven Aircraft”, Journal of Aircraft 52(6) 2011 p2172 – 2174 (2015)
39. Catalano F.M., “On the Effects of an Installed Propeller Slipstream on Wing Aerodynamic Characteristics”, Acta Polytechnica Vol. 44 No. 3/2004
40. D.P. Raymer, “Aircraft Design: A Conceptual Approach’ Third Edition, AIAA Reston, Virginia, ISBN 1-56347-281-0 (1999)
41. ESDU 94044.Excrescence drag levels on aircraft. ESDU International. November 2007
42. Turns S.R., “Thermal-Fluid Sciences”, Cambridge University Press, Cambridge (2012)
43. ESDU 73016. The mean skin friction coefficient for a rough flat plate with a turbulent two-dimensional boundary layer in compressible adiabatic flow, with application to wedges, cylinders and cones. ESDU International. 1973

LIST OF FIGURES

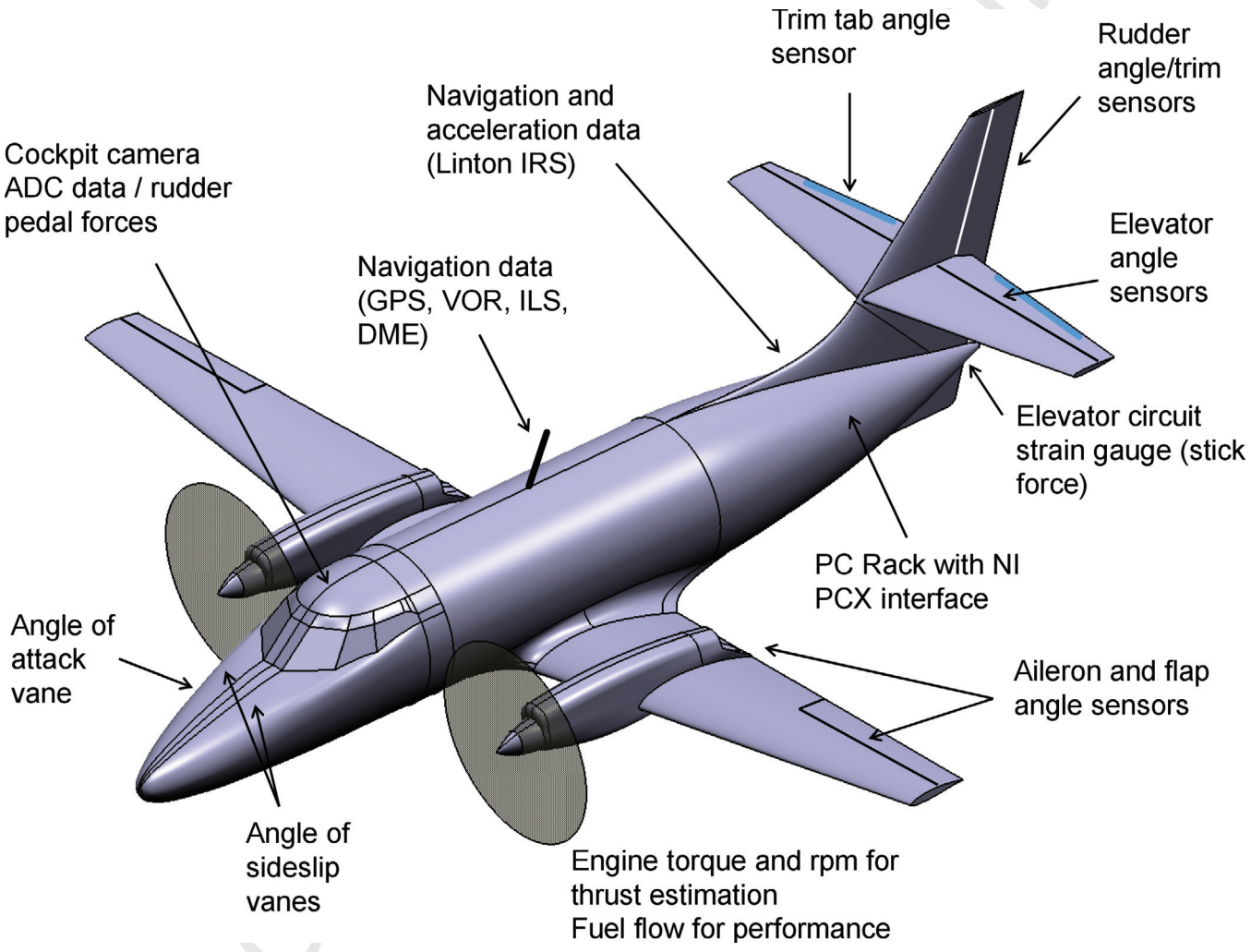

Fig1

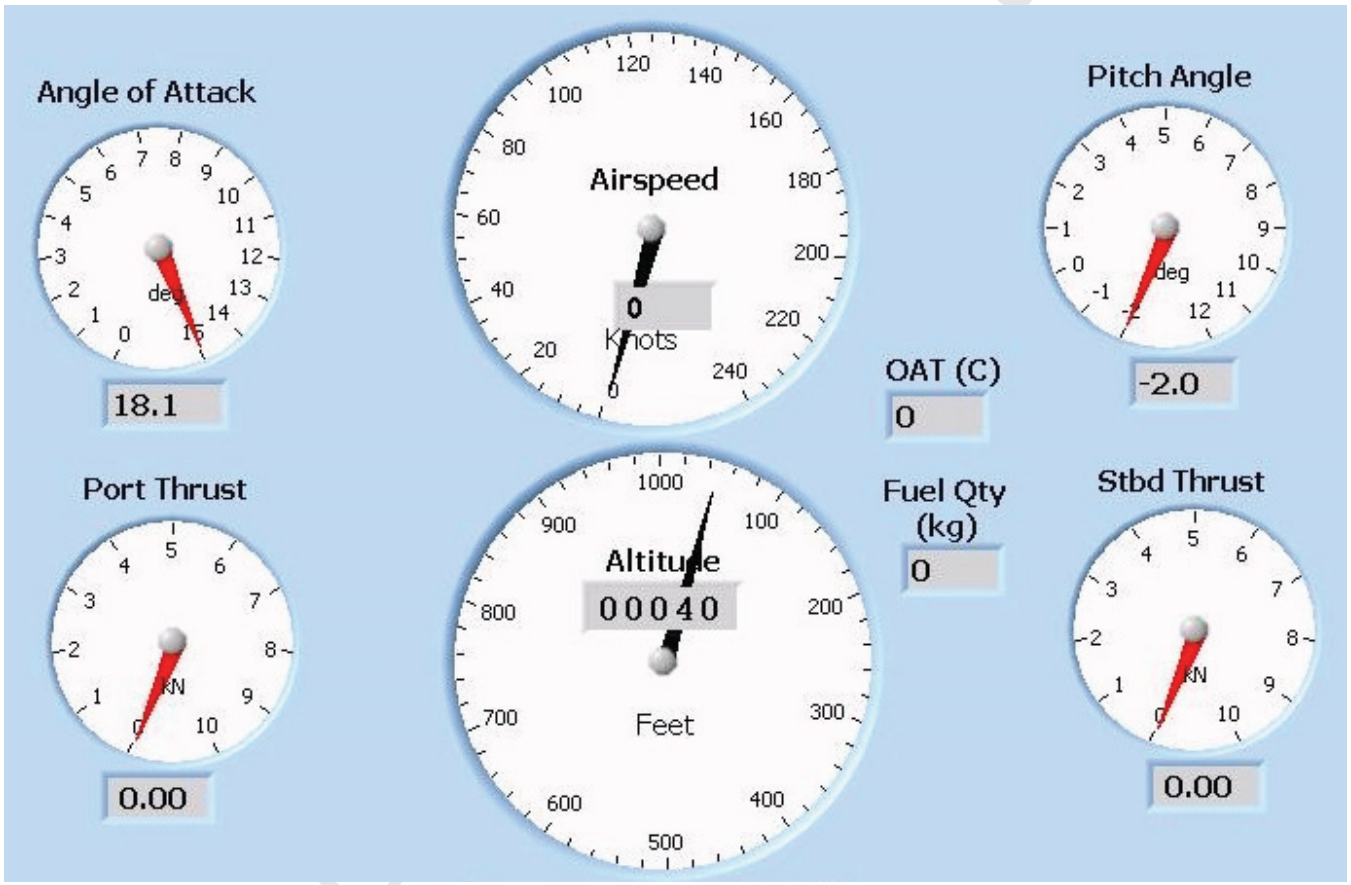

Fig2

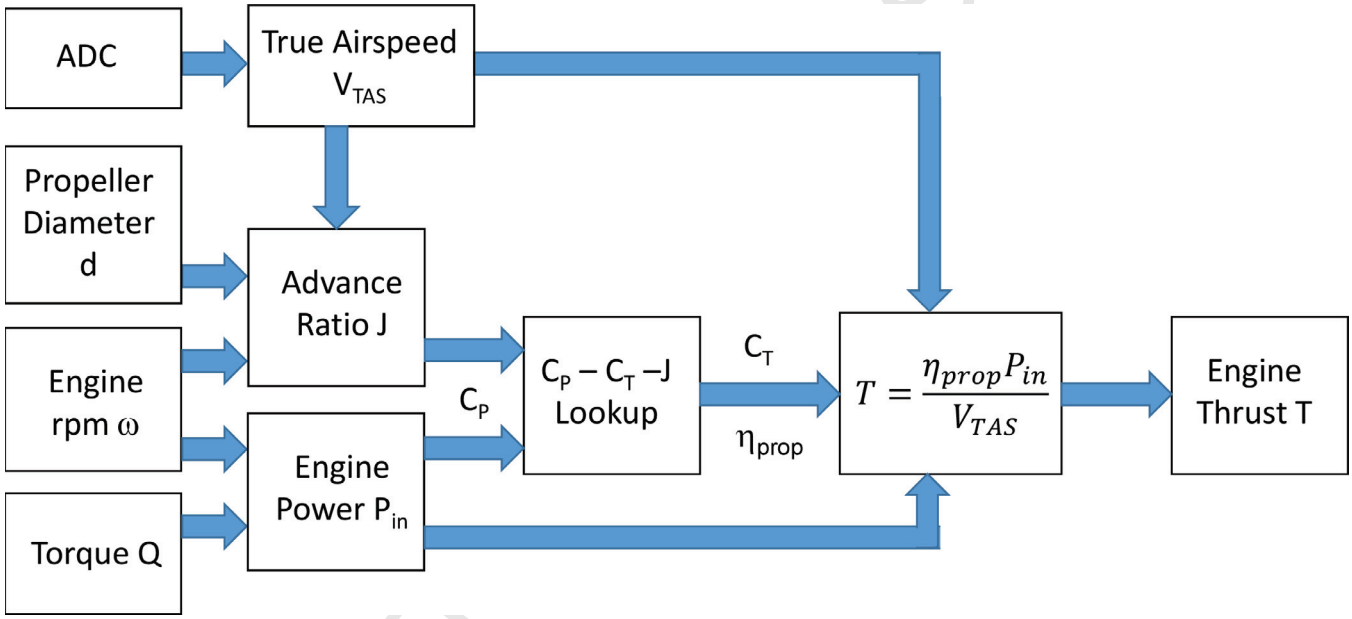

Fig3

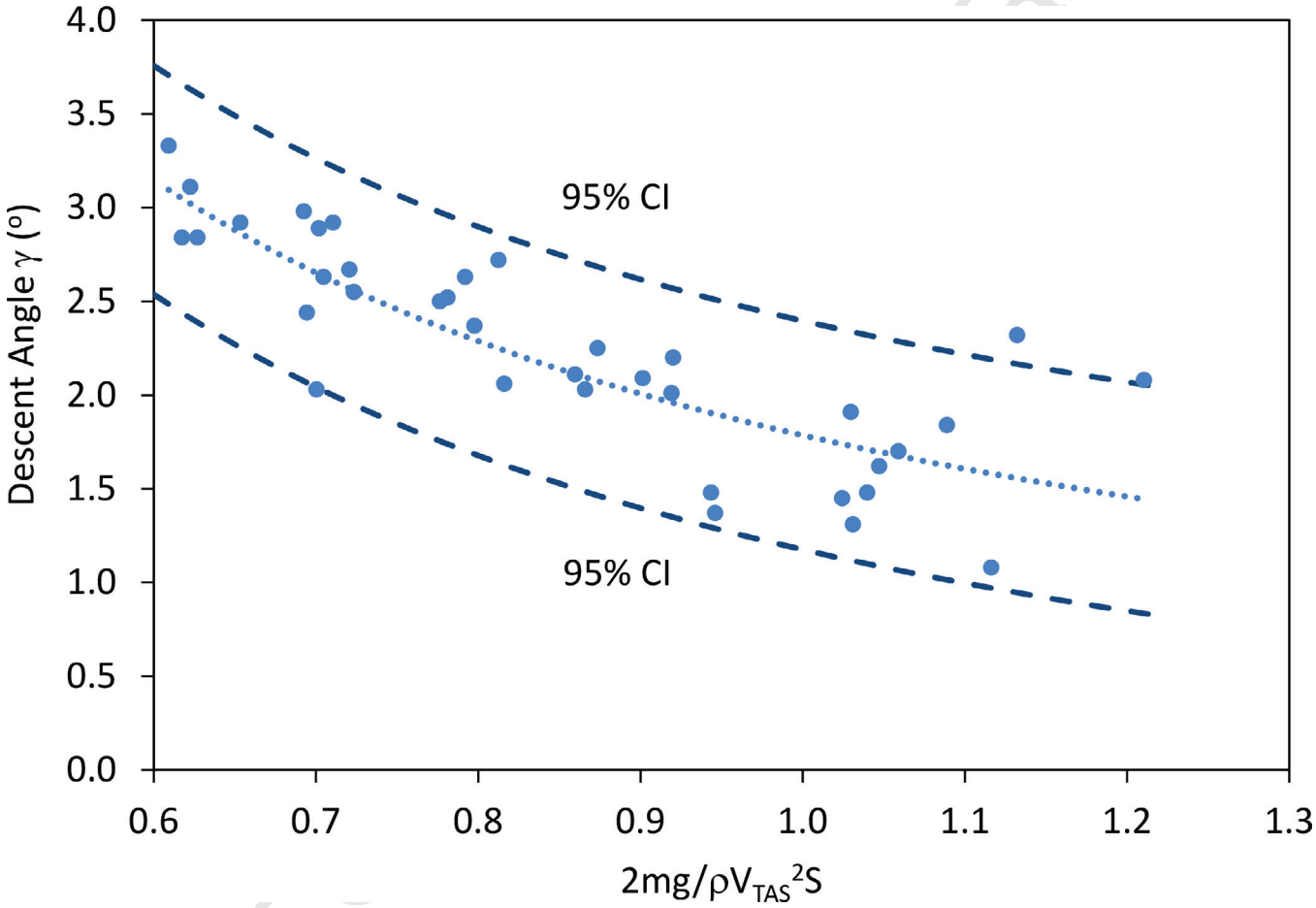

Fig4

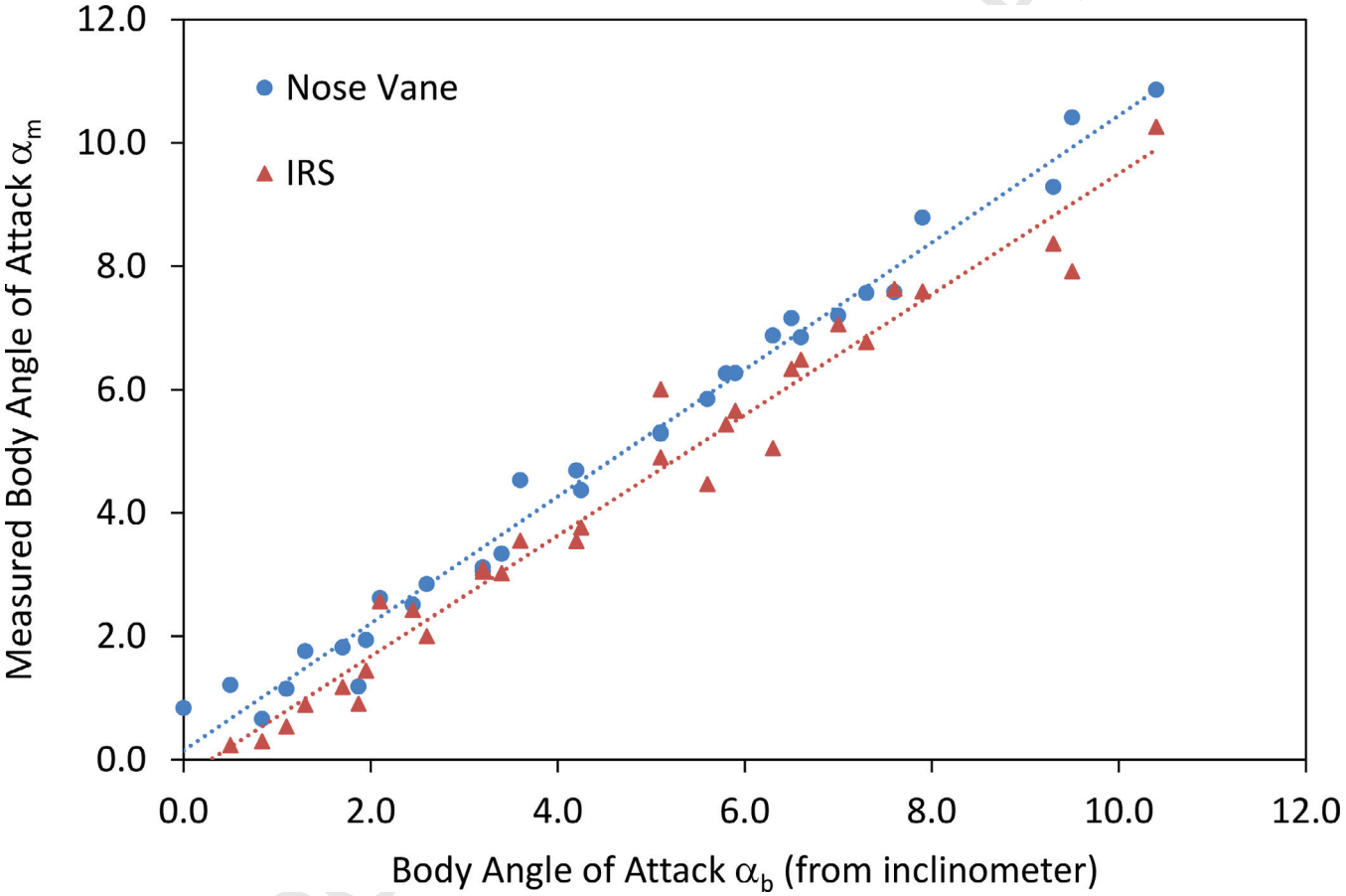

Fig5

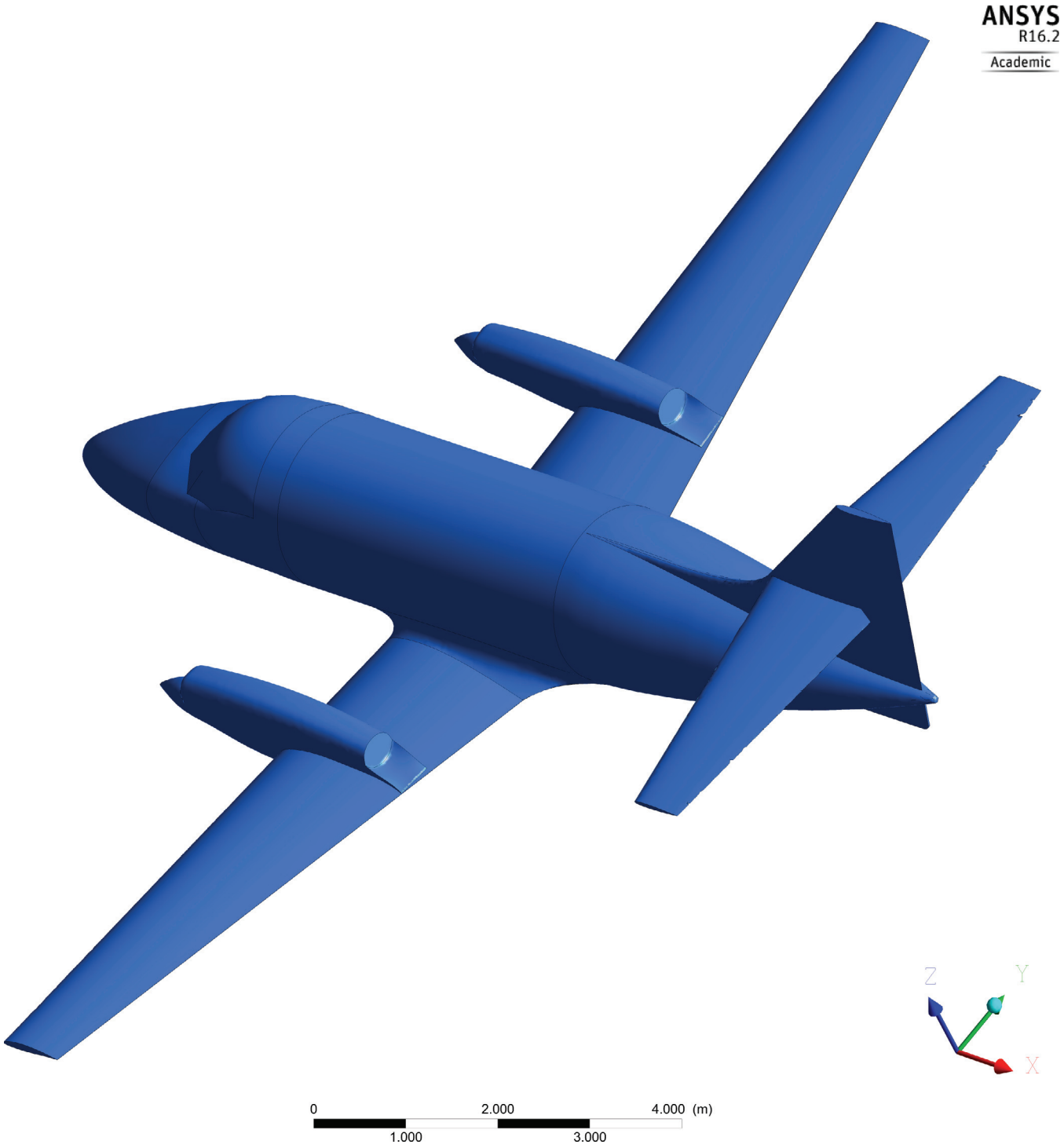

Fig6_1

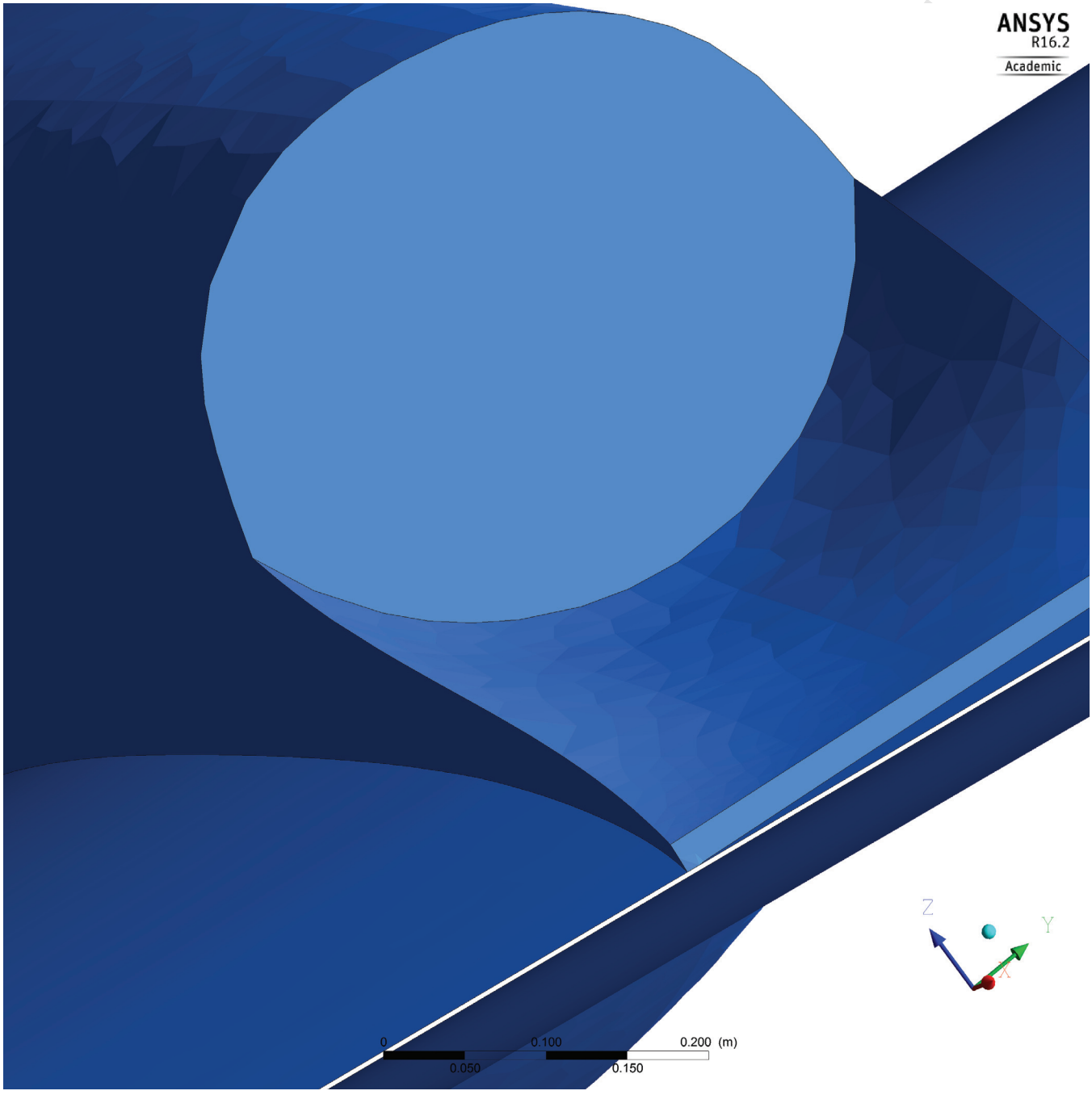

Fig6_2

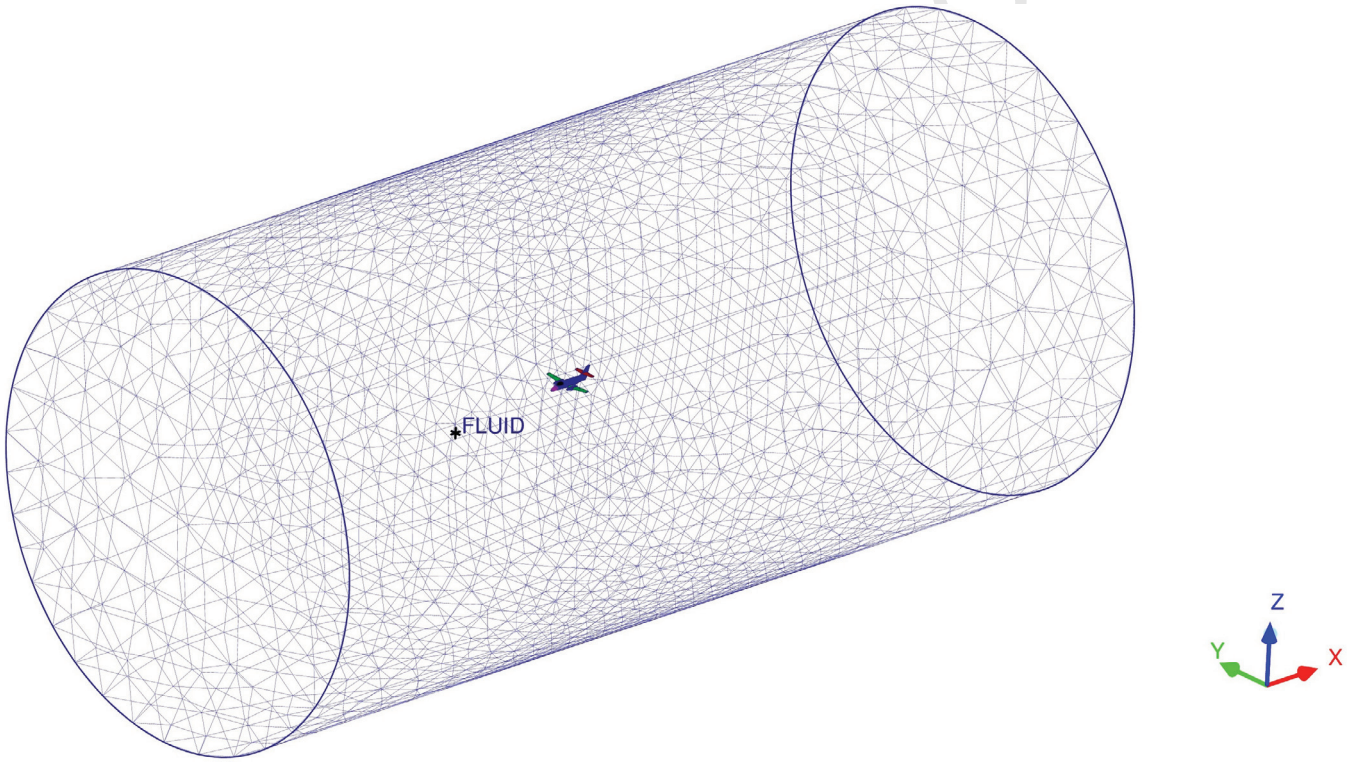

Fig7_1

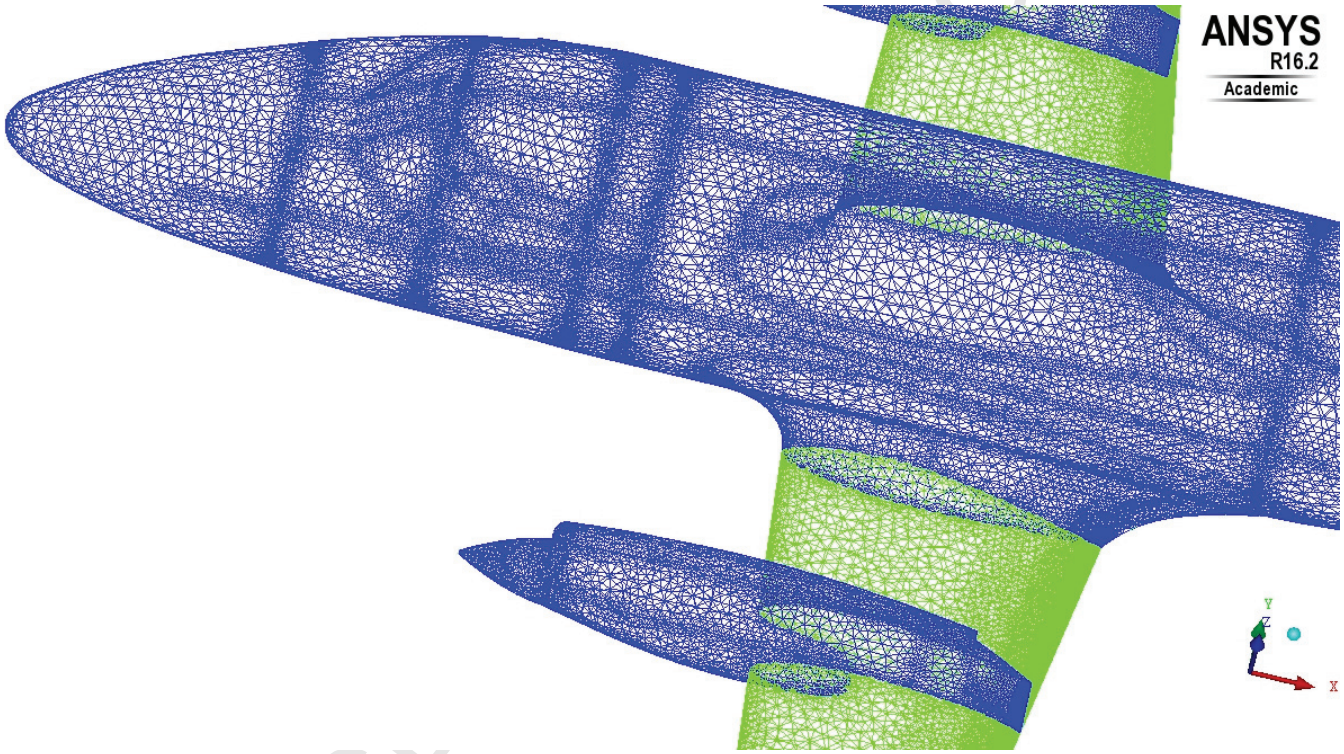

Fig7_2

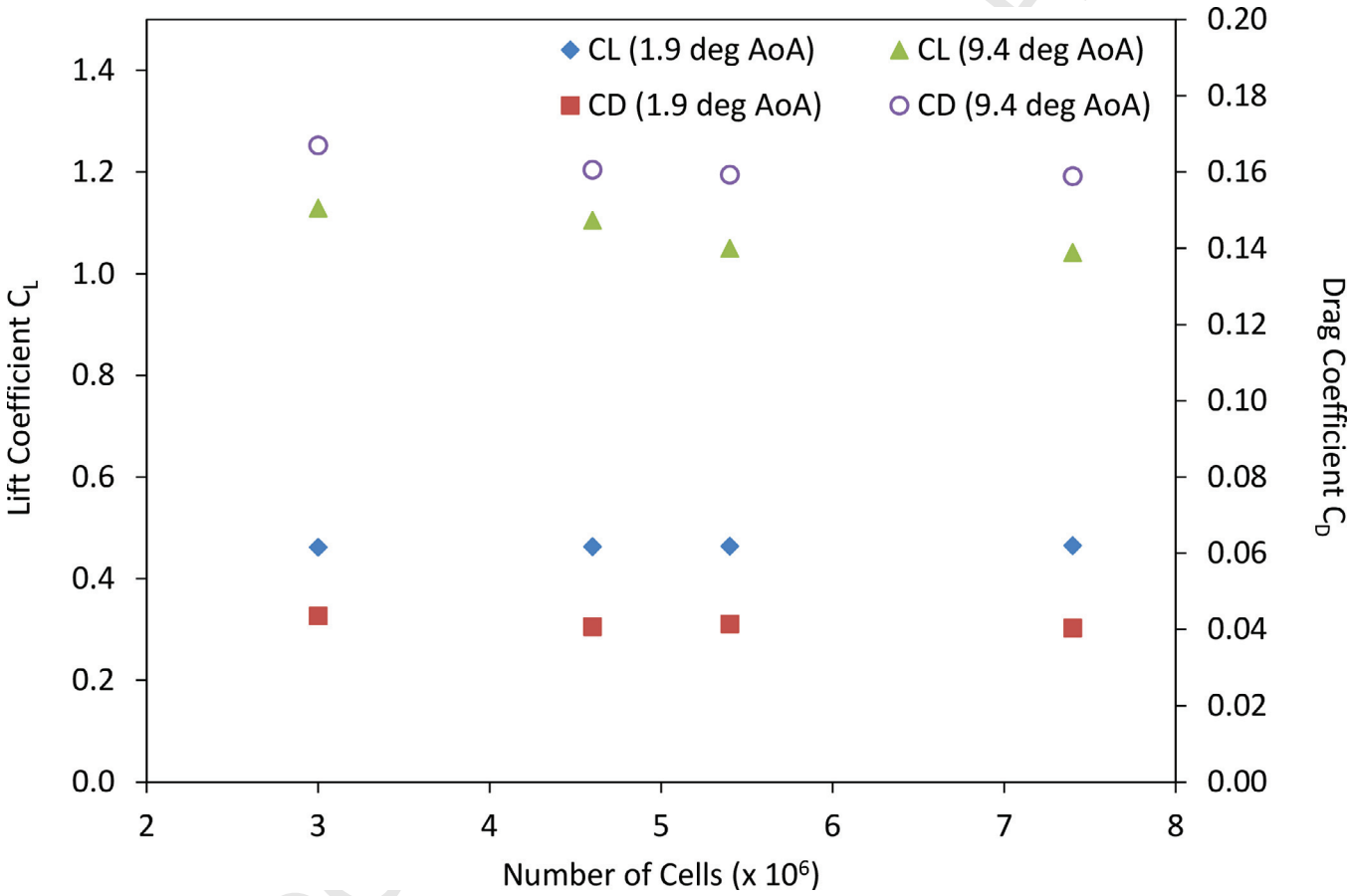

Fig8

Fig9

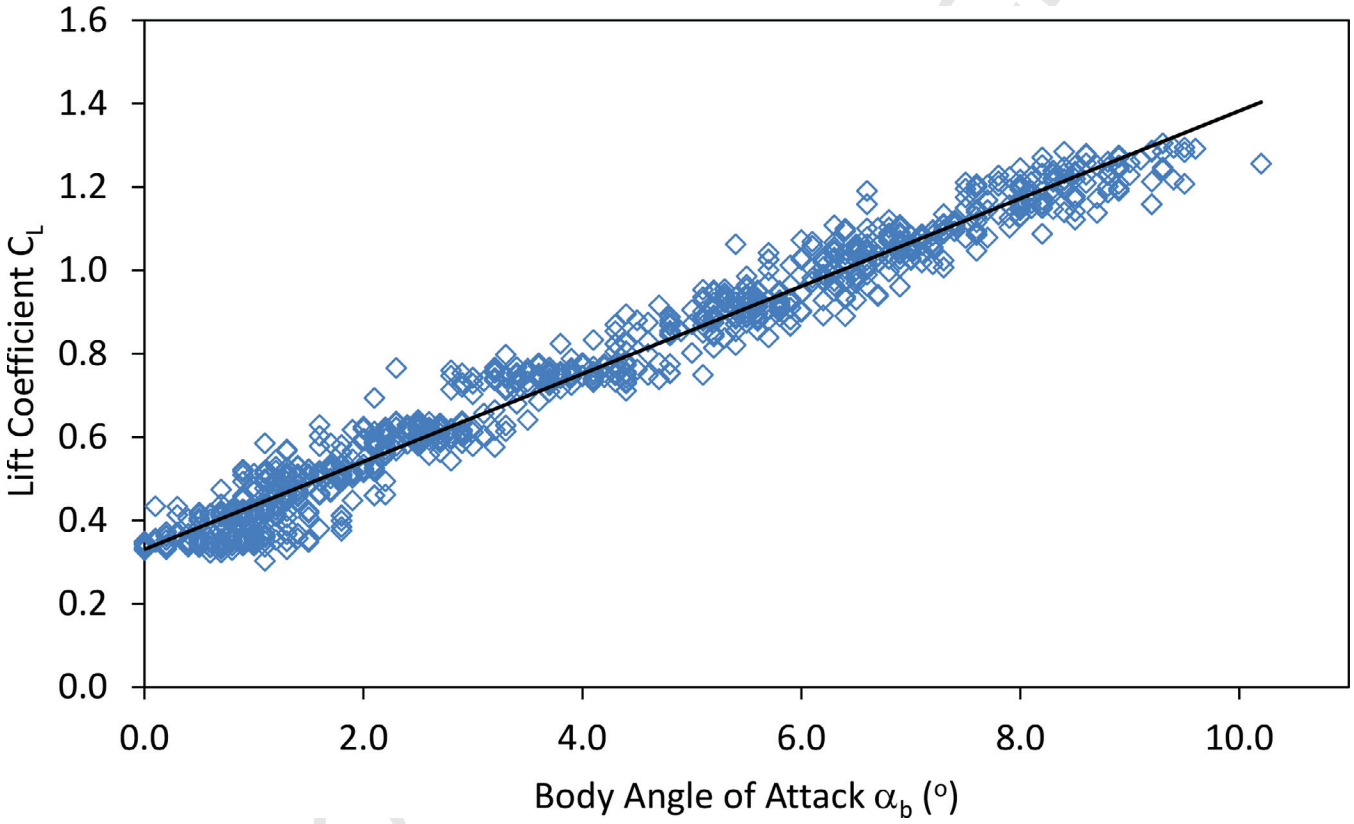

Fig10

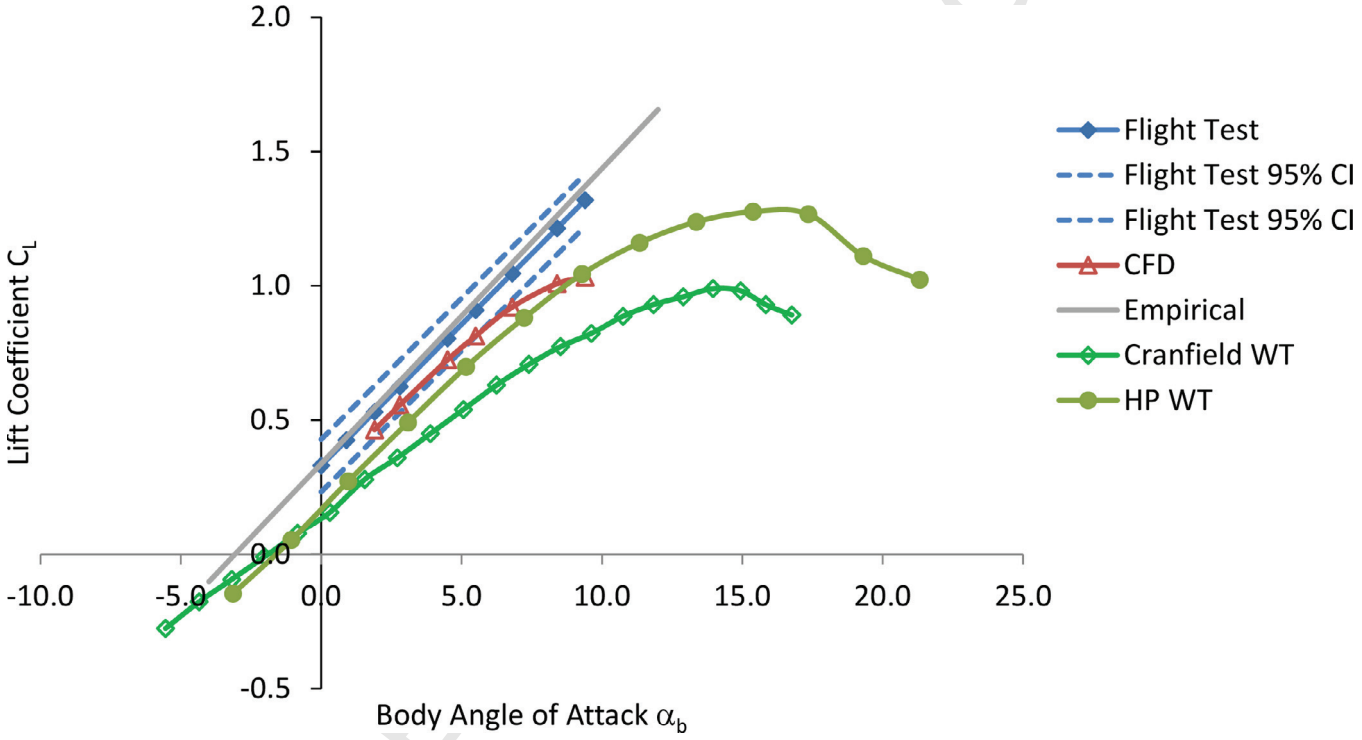

Fig11

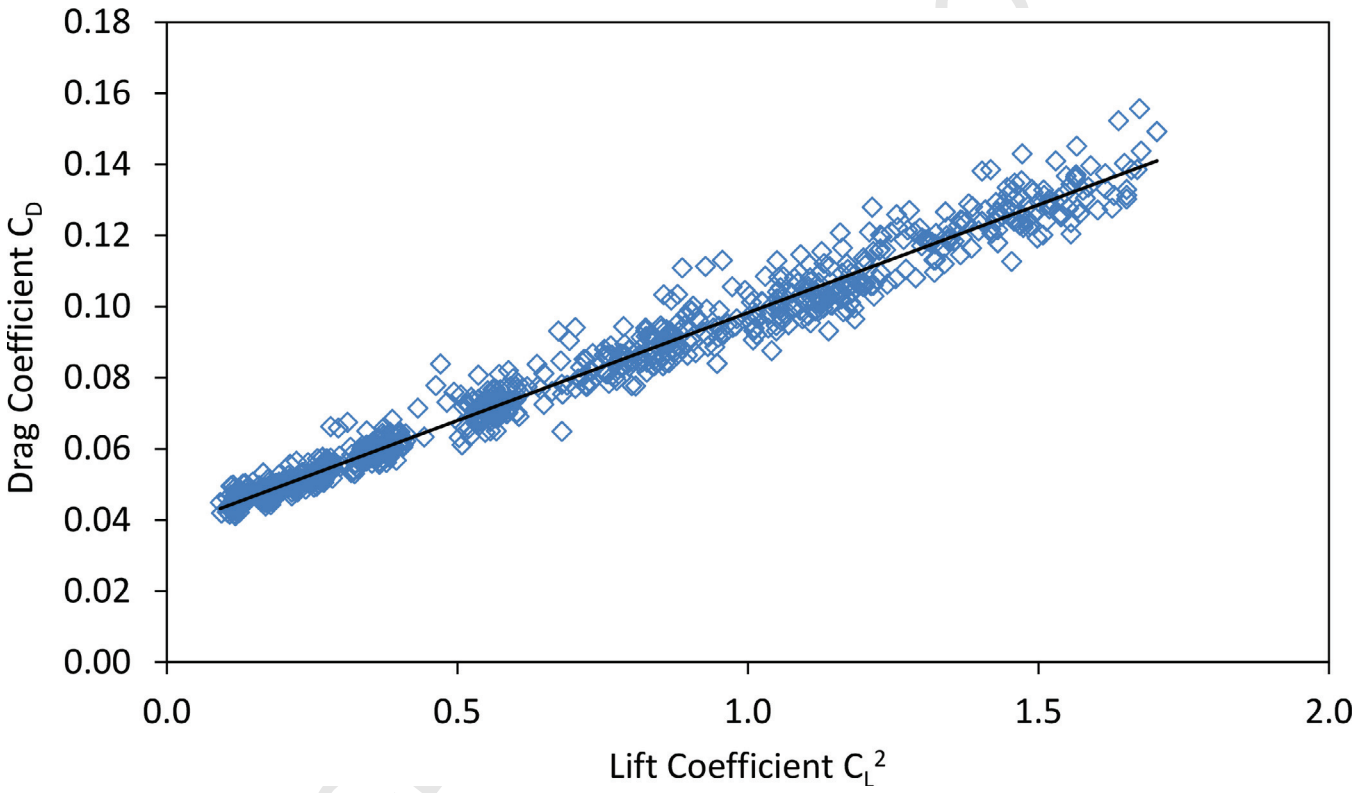

Fig12

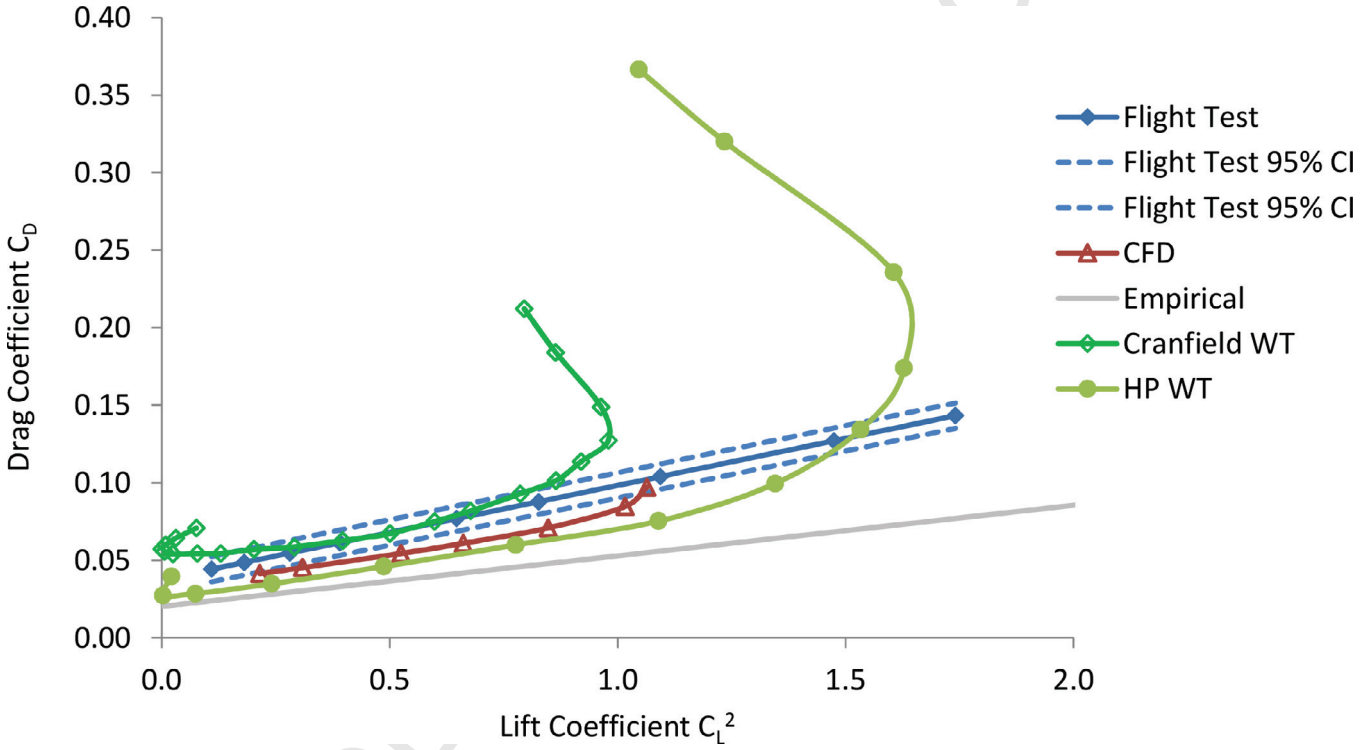

Fig13

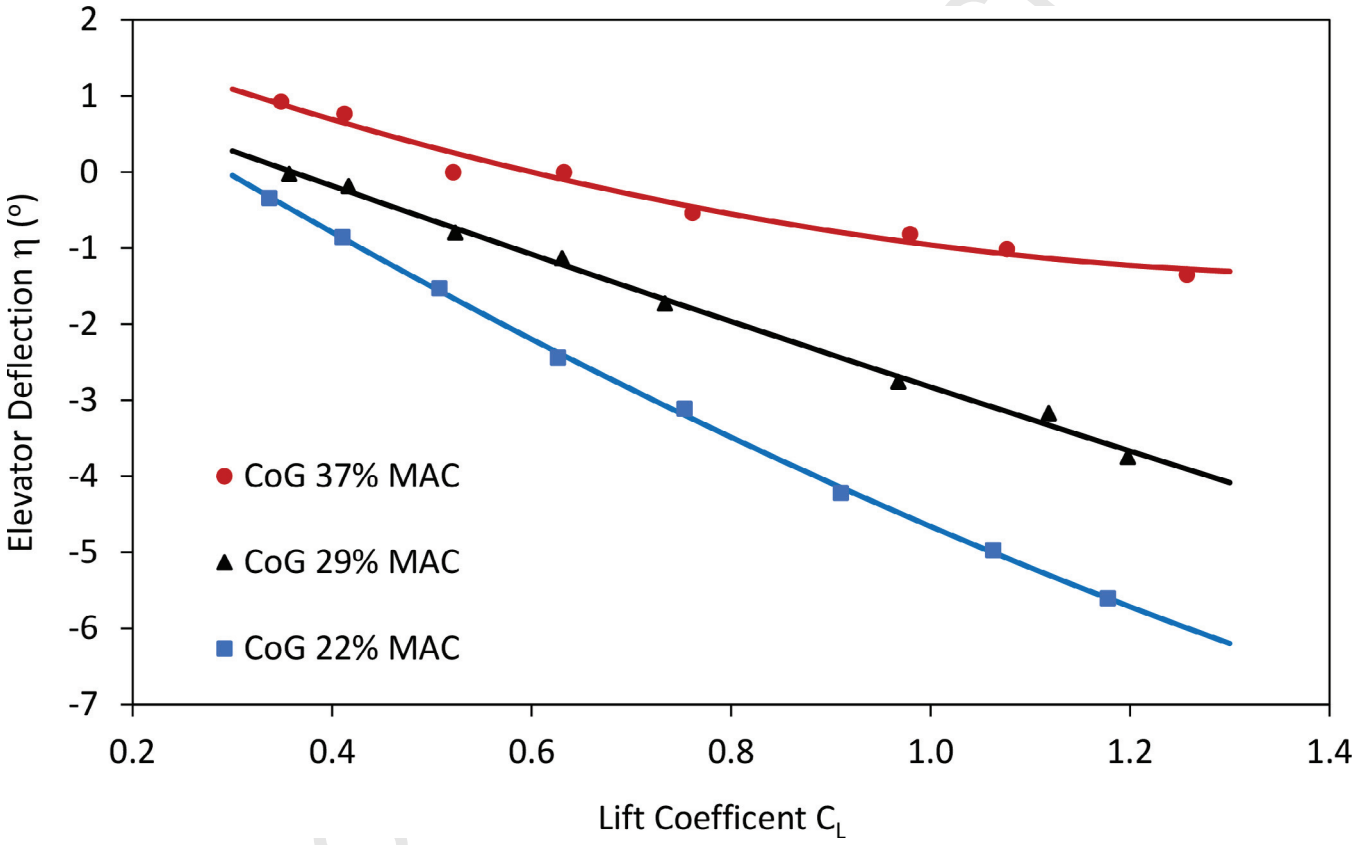

Fig14